Atmos. Chem. Phys. Discuss., 14, 9975–10024, 2014
www.atmos-chem-phys-discuss.net/14/9975/2014/
doi:10.5194/acpd-14-9975-2014

Atmospheric Chemistry and Physics Discussions

Variability of tropospheric methane above the Mediterranean Basin inferred from satellite and model data

P. Ricaud[1], B. Sič[1], L. El Amraoui[1], J.-L. Attié[1,2], P. Huszar[3], S. Szopa[4], J. Parmentier[1], N. Jaidan[1], M. Michou[1], R. Abida[1], R. Zbinden[1], F. Carminati[1,2,5], D. Hauglustaine[4,6], T. August[7], J. Warner[5], R. Imasu[8], N. Saitoh[9], and V.-H. Peuch[10]

[1]CNRM-GAME, Météo-France/CNRS UMR3589, Toulouse, France
[2]Université de Toulouse, Laboratoire d'Aérologie, CNRS UMR5560, Toulouse, France
[3]Department of Meteorology and Environment Protection, Faculty of Mathematics and Physics, Charles University, Prague, V Holešovičkách 2, Prague 8, 18000, Czech Republic
[4]Laboratoire des Sciences du Climat et de l'Environnement, CNRS UMR1572, Gif sur Yvette, France
[5]University of Maryland, College Park, Maryland, USA
[6]Laboratoire Image Ville Environnement, CNRS UMR7362, Strasbourg, France
[7]EUMETSAT, Darmstadt, Germany
[8]University of Tokyo, Tokyo, Japan
[9]Center for Environmental Remote Sensing, Chiba University, Japan

[10]European Centre for Medium-Range Weather Forecasts, Reading, UK

Received: 25 March 2014 – Accepted: 7 April 2014 – Published: 17 April 2014

Correspondence to: P. Ricaud (philippe.ricaud@meteo.fr)

Published by Copernicus Publications on behalf of the European Geosciences Union.

ACPD
14, 9975–10024, 2014

Abstract

The space and time variabilities of methane (CH_4) total column and upper tropospheric mixing ratios are analyzed above the Mediterranean Basin (MB) as part of the Chemical and Aerosol Mediterranean Experiment (ChArMEx) programme. Spaceborne measurements from the Thermal And Near infrared Sensor for carbon Observations-Fourier Transform Spectrometer (TANSO-FTS) instrument on the Greenhouse gases Observing SATellite (GOSAT) satellite, the Atmospheric InfraRed Spectrometer (AIRS) on the AURA platform and the Infrared Atmospheric Sounder Interferometer (IASI) instrument aboard the MetOp-A platform are used in conjunction with model results from the Chemical Transport Model (CTM) MOCAGE, and the Chemical Climate Models (CCMs) CNRM-AOCCM and LMDz-OR-INCA (according to different emission scenarios). In order to minimize systematic errors in the spaceborne measurements, we have only considered maritime pixels over the MB. The period under interest spans from 2008 to 2011 considering satellite and MOCAGE data and, regarding the CCMs, from 2001 to 2010. An East-West gradient in CH_4 is observed and modelled whatever the season considered. In winter, air masses mainly originating from Atlantic Ocean and Europe tend to favour an elevated amount of mid-to-upper tropospheric CH_4 in the West vs. the East of the MB, with a general upward transport above the MB. In summer, the meteorological state of the MB is changed, favouring air from Northern Africa and Middle East together with Atlantic Ocean and Europe, with a general downward motion above the MB. The Asian Monsoon traps and uplifts high amounts of CH_4 that are transported towards North Africa and Middle East by the Asian Monsoon Anticyclone to finally reach and descent in the East of the MB. Consequently, the mid-to-upper tropospheric CH_4 is much greater in the East than in the West of the MB. The seasonal variation of the difference in CH_4 between the East and the West MB does show a maximum in summer for pressures from 500 to 100 hPa considering both spaceborne measurements and model results whatever the emission scenarios used. From this study, we can conclude that CH_4 in the mid-to-upper troposphere over the MB

ACPD
14, 9975–10024, 2014

is mainly affected by long-range transport, particularly intense in summer from Asia. In the low-to-mid troposphere, the local sources of emission in the vicinity of the MB mainly affect the CH_4 variability.

1 Introduction

Recent years have been marked by concerns on the impact and the role that trace gases play in climate and air pollution changes. The ongoing changes of our atmosphere (composition, climate, air pollution, radiation) are very well documented (IPCC, 2007). Trace gases like methane (CH_4), carbon dioxide (CO_2), carbon monoxide (CO), nitrous oxide (N_2O) play an important role in atmospheric change because their concentrations are strongly influenced by human activities. Knowledge of today's CO_2, CH_4 and N_2O sources and sinks, their spatial distribution and their variability in time is essential for predicting the future of the Earth's climate (IPCC, 2007).

The net positive impact of the human activity on climate, starting from 1750, has been evaluated to 1.6 [+ 0.6 to +2.4] $W m^{-2}$ (IPCC, 2007). In the atmosphere, the long-lived greenhouse gases account for $2.63 \pm 0.26\,W m^{-2}$ and are the predominant radiative terms. CO_2, with tropospheric lifetime of 30–95 years, has a radiative efficiency of $1.4 \times 10^{-5}\,W m^{-2}\,ppb^{-1}$, but CH_4 and N_2O, with tropospheric lifetimes of 12 and 114 years, respectively, are intensely more efficient by 3.7×10^{-4} and $3.03 \times 10^{-3}\,W m^{-2}\,ppb^{-1}$, respectively. IPCC (2007) estimated CH_4 and N_2O to be responsible of 0.48 [+0.43 to 0.53] and 0.16 [+0.14 to 0.18] $W m^{-2}$, respectively in the radiative forcing changes.

Long-lived species (CO_2, CH_4, and N_2O) are believed to be very well-mixed and evenly distributed throughout the lower atmosphere. Conversely, shorter-lived gases, like CO with a lifetime of a few months in the troposphere, are believed to have concentrations that are very variable in both, spatial and temporal ways, and they are more concentrated in the lowermost part of the atmosphere, closer to their sources. Beside this, it is known that all gases could have different regional climate responses due to

ACPD
14, 9975–10024, 2014

regional particularities and differences, but also because there is a strong link between regional and global climate (Ramanathan and Carmichael, 2008).

It is rather challenging to measure long-lived species from space focusing on tropospheric layers. The past/present nadir-viewing instruments having the capabilities to actually measure long-lived species in the troposphere have been/are: the Interferometric Monitor for Greenhouse gases (IMG) instrument operating in the Thermal Infrared (TIR) domain aboard the ADvanced Earth Observing Satellite (ADEOS-1) platform in 1996–1997 (Clerbaux et al., 1998) detecting CO_2, CH_4 and N_2O; the near-IR (NIR) Scanning Imaging Absorption Spectrometer for Atmospheric Chartography (SCIAMACHY) aboard the ENVIronment SATellite (ENVISAT) platform (Buchwitz et al., 2000) detecting CO_2 and CH_4 from 2002 to 2012; the Tropospheric Emission Spectrometer (TES) operating in the TIR aboard the Aura platform detecting CH_4 (Worden et al., 2012) from 2004 to date; the Thermal And Near infrared Sensor for carbon Observations – Fourier Transform Spectrometer (TANSO-FTS) on the Greenhouse gases Observing SATellite (GOSAT) platform (Yokota et al., 2009) both in the Short-Wave InfraRed (SWIR) and in the TIR detecting CH_4 and CO_2 from 2008 to date; the Atmospheric InfraRed Sounder (AIRS) aboard the Aqua platform (Xiong et al., 2008) measuring CH_4 in the TIR from 2004 to date; the Infrared Atmospheric Sounding Interferometer (IASI) instrument aboard the MetOp-A and –B platforms (Hilton et al., 2012) detecting CH_4, CO_2 and N_2O in the TIR from 2008 to date; and the future dedicated CO_2 mission Orbiting Carbon Observatory–2 (OCO-2) operating in the SWIR to be launched in 2014 (Crisp et al., 2004).

The sensitivity of the TIR to measure CH_4 and CO_2 is rather weak except on areas showing a high thermal contrast at the surface (vertical gradient between the surface temperature and the temperature in the planetary boundary layer) as the ones encountered during heatwave periods or over the tropics (see e.g. Crevoisier et al., 2009 and 2013 for CH_4) contrarily to the measurements performed in the SWIR (see e.g. GOSAT measurements of CO_2 and CH_4, Yoshida et al., 2013). In parallel to the satellite data, models have also been used in order to assess the variability, sources and sinks, and

ACPD
14, 9975–10024, 2014

future trends of the long-lived species. Examples are: CH_4 and CO_2 emission and flux estimates at global scales (Bergamaschi et al., 2009; Bousquet et al., 2011), future evolution of long-lived species included in the international Atmospheric Chemistry and Climate Model Intercomparison initiative involving more than 10 different models (Lamarque et al., 2013), etc. Long-lived species can also be used to diagnose transport processes in the troposphere. Considering IASI N_2O total columns, recent studies (Ricaud et al., 2009) have shown that the N_2O longitudinal distribution was non uniform in the equatorial band. Coupled with the 3-D Chemical-Transport Model (CTM) MOCAGE from Météo-France, the inhomogeneity in the three-month averaged N_2O fields was attributed to the impact of the tropical Walker cells converging towards the African continent and diverging from the Maritime and South American continents.

The ChArMEx (Chemistry and Aerosol Mediterranean Experiment) Project (http://charmex.lsce.ipsl.fr/) is the atmospheric chemistry component of a large multidisciplinary Mediterranean regional program proposed by France. It intends, among other objectives, to quantify processes explaining the temporal evolution of chemical compounds and aerosols in the troposphere above the Mediterranean Basin (MB). To achieve these goals, the program uses a large set of data (satellites, ground-based, sondes, aircraft, models and assimilation) in order to (1) estimate the variabilities and recent trends of several species (e.g. O_3, CO, N_2O, etc.) and aerosols, (2) evaluate the synoptic-scale circulation that controls their transport, and (3) estimate the future chemical climate over the MB by 2100.

Numerous studies have examined the variabilities of atmospheric compounds above the MB to highlight the processes (sources and sinks) associated by coupling surface, balloon-borne, airborne, spaceborne measurements with models results at different scales, from mesoscales to global scales. Constituents are for instance aerosol (Nabat et al., 2012), radionuclides (Masson et al., 2010), ozone (Liu et al., 2009), carbon monoxide (Drori et al., 2012), etc. The impact of the different meteorological regimes together with the seasonal variabilities of the emissions of various atmospheric constituents, e.g. CO emitted from fires in summers, produce a seasonal variation in all

ACPD
14, 9975–10024, 2014

the constituents, but also, a longitudinal gradient between the Eastern and the Western parts of the MB, together with a seasonal variation in the gradient. For example, European anthropogenic emissions were found to significantly influence the Eastern MB surface CO concentrations, while European biomass burning emissions were found to have only a small impact on Eastern MB surface CO concentrations (Drori et al., 2012).

The present study mainly focuses on the CH_4 variability above the MB to (1) assess the seasonal variability and (2) attribute the variability to different processes at both meso and global scales depending on the season and the altitude layer considered. Our approach is based on three models: the CTM MOCAGE (Josse et al., 2004) and the two Chemical Climate Models (CCMs) CNRM-AOCCM from Météo-France (Huszar et al., 2013) and LMDz-OR-INCA (Hauglustaine et al., 2004; Szopa et al., 2013) from the Laboratoire des Sciences du Climat et de l'Environnement (LSCE). To complete, we have considered the CH_4 profiles from AIRS and GOSAT, and the CH_4 total columns from IASI.

The manuscript is structured as follow. In Sect. 2, we present the spaceborne instruments and datasets involved in this study, namely MetOp-A/IASI, AQUA/AIRS and GOSAT/TANSO together with the models, namely MOCAGE, CNRM-AOCCM and LMDz-OR-INCA. The meteorology and climatology of CH_4 inferred from the different datasets above the MB are discussed in Sect. 3. The CH_4 variability both in the East and in the West of the MB is presented in Sect. 4. A detailed discussion of the different processes involved in the CH_4 variability above the MB is presented in Sect. 5. Finally, Sect. 6 concludes the paper.

2 The datasets

2.1 The satellite data

We have concentrated our analysis on CH_4 as measured by three different spaceborne TIR sensors (IASI, AIRS and GOSAT) by only considering the pixels over the Mediter-

ACPD
14, 9975–10024, 2014

ranean Sea in order to minimize the systematic biaises among pixels (day vs. night, land vs. sea). Maritime pixels are the least contaminated pixels by surface emissivity which, on the land, could have important impact on the retrieved value. Surface emissivity on the sea should be a lot smaller and spatially a lot more uniform than compared to land emissivity. Measurements over land could also have a different sensitivity depending on the surface type that makes retrieval more difficult (see e.g. Claeyman et al., 2011). Different types of surfaces have different emissivities and reflectivities that impact on the retrievals. Also the amplitude of the diurnal variation of surface temperature is less intense over the sea than over the continent, that is to say the sensitivity of the IR measurements over the sea during day and night is somewhat consistent and concentrated in the mid-troposphere although the sensitivity of land IR nadir measurements is, on average, lower during the day than during the night depending on the actual value of the thermal contrast at the surface (e.g. Claeyman et al., 2011).

Infrared sounders measurement errors can be rather large, e.g. up to 10 % or more for a single CH_4 total column IASI pixel (Turquety et al., 2004). We thus need a large number of measurements to reduce random error and uncertainty. To obtain more than a thousand measurements, it is necessary to make seasonally/monthly averages of data. By this mean, we can lower the random error to less than 1 %. Systematic errors, if any, will of course be unchanged. It is the main reason why, in our analysis, we use a differential method to highlight the variability of the CH_4 fields by considering the difference between the Eastern MB (EMB) and the Western MB (WMB), assuming that the systematic errors are of the same order of magnitude (although partially unknown) within each geographical box. Also, note that we have used the tropopause height and pressure fields provided by the National Oceanic and Atmospheric Administration (NOAA) National Centers for Environmental Prediction (NCEP) reanalyses.

2.1.1 The IASI data

IASI is an IR instrument onboard the space platform MetOp-A launched by the European Organisation for the Exploitation of Meteorological Satellites (Eu-

ACPD
14, 9975–10024, 2014

metsat) in 2006 (see e.g., http://smsc.cnes.fr/IASI; http://www.eumetsat.int/Home/Main/Satellites/Metop/Instruments/SP_2010053151047495). The platform has a sun-synchronous polar orbit inclined 98.7° to the Equator crossed (descending node) at 09:30 Local Solar Time (LST), at the altitude of about 815 km. The time for an orbit is 101 min with a repeat cycle of 29 days. The cross-track angle of sight is ±48.3°, each measurement of 2 × 2 pixels corresponds to a circular pixel of 12 km diameter at sub-satellite point. Based on Michelson interferometer, IASI is an accurately calibrated Fourier Transform Spectrometer probing the atmosphere in the 3.6–15.5 µm spectral range with 8461 spectral channels and a spectral sampling of 0.25 cm^{-1} and resolution of 0.5 cm^{-1} after apodisation. Within the spectral domain covered by IASI, a number of atmospheric constituents can be measured including H_2O, O_3, CO_2, N_2O, CH_4, and CO. The retrieval algorithm for CH_4 is a feed-forward artificial neural network adapted from Turquety et al. (2004). The retrieval method is embedded in the operational IASI Level 2 product processing facility at EUMETSAT (EUMETSAT, 2004; Schlüssel et al., 2005; August et al., 2012). From the spectral bandwidth 1 230–1 347 cm^{-1}, the estimated accuracy of the CH_4 total column is about 2 % and the estimated precision is of the order of 10 % (Turquety et al., 2004). As for the accuracy, the value of 2 % refers to the retrieved values from a synthetic data set (spectra calculated via radiative transfer simulations and instrument noise characteristics from assumed atmospheric states) and does not account for errors in the radiative transfer (RT) simulations (e.g. neglecting of Non-Local Thermodynamic Equilibrium effects, errors in spectroscopy, and errors due to truncated RT modelling). The true accuracy cannot be stated without reference to independent means of comparison, which are not available so far. Consequently, in the present study, we consider a random Gaussian error of ∼ 10 % associated to each single pixel of retrieved total column of CH_4. The vertical sensitivity of the total column CH_4 is peaking at 8 km with a width at half maximum from about 4 to 14 km (Razavi et al., 2009) at mid-latitudes, that is to say a sensitivity in the mid-troposphere. Geophysical level 2 pre-operational data are provided by EUMETSAT (from version 4 to version 5 from 2008 to 2011). The methane products have not been validated and are

ACPD
14, 9975–10024, 2014

not operational. They are experimental products, routinely generated for demonstration and evaluation. The number of daily total columns of CH_4 averaged in a $1^\circ \times 1^\circ$ bin is highly variable because only IASI data without cloud contamination in the line of sight are used along the large 2200 km swath of the scan.

2.1.2 The AIRS data

AIRS is an IR instrument onboard the space platform NASA EOS Aqua launched in 2002 (see: http://airs.jpl.nasa.gov/). Together with the Advanced Microwave Sounding Unit (AMSU) and the Humidity Sounder for Brazil, they form an integrated cross-track scanning temperature and humidity sounding system. The platform has a sun-synchronous polar orbit with 14 orbits per day and equatorial crossing at 13:30 LST ascending node, at the altitude of about 705 km. The cross-track angle of sight is $\pm 49^\circ$, with a resolution of 13.5 km at nadir and 41 km × 21.4 km at the scan extremes (Aumann et al., 2003). The AIRS 2 378 channels range 649–1136, 1217–1613 and 2169–2674 cm^{-1} at high spectral resolution ($\lambda/\Delta\lambda \sim 1200$). In the current retrieval system, AMSU is combined with AIRS to retrieve the atmospheric temperature-humidity profiles, cloud and surface properties, and minor gases in a 45 km Field-Of-View. AIRS measures approximately 200 channels in the 7.66 µm absorption band of CH_4, of which 71 channels are used to retrieve CH_4. A detailed description of the retrieval algorithm can be found in Susskind et al. (2011). We have also considered the averaging kernels provided by NASA in order to degrade the vertical resolution of the model outputs. In the tropics and mid-latitudes, the most sensitive layer of AIRS channels to CH_4 is at about 200–300 hPa, and it decreases to about 400–500 hPa in the polar region. Moreover, the sensitivity in the polar region is usually smaller than in the midlatitude and tropics. In the 200–300 hPa layer, considering the version V5 used in the present analysis (Xiong et al., 2008), the precision of AIRS CH_4 is estimated to be 30 ppbv (1.7 %) and validation using in situ aircraft measurements shows that the accuracy of the retrieved CH_4 is 0.5–1.6 %. Daily maritime profiles of CH_4 have been averaged in $1^\circ \times 1^\circ$ bins over the MB.

ACPD
14, 9975–10024, 2014

2.1.3 The GOSAT data

The Japanese Aerospace Exploration agency (JAXA) launched the GOSAT platform in 2009, with the TANSO-FTS spectrometer which operates in the TIR and SWIR domains (Kuze et al., 2009). It is designed for greenhouse gases research, CO_2 and CH_4. The spectrometer is a nadir-viewing instrument sensitive to 0.7–14.3 µm radiation. On the GOSAT orbit at about 650 km altitude, the instrument makes swath up to 800 km wide and one measurement has an horizontal resolution of 10.5 km. In the SWIR domain (Yokota et al., 2009), CH_4 mixing ratios are retrieved in the 1.67 µm CH_4 absorption band using the optimal estimation method (Rodgers, 2000). We have first used the CH_4 total columns from SWIR channels corresponding to the spring and summer 2010 seasons (L2 version 1.3 and L3 version 1.4) by only considering pixels over the Mediterranean Sea. Unfortunately, the sensitivity of the SWIR measurements at mid-latitudes over the sea is very weak for CH_4, thus few meaningful pixels could have been retrieved preventing the use of such information in our analysis. The TIR measurements from Band 4 (5.5–4.3 µm) provide vertical profiles of CH_4 along 7 vertical levels (Imasu et al., 2007) by using the optimal estimation method. A selection by using Degree of Freedom of Signal (DFS) is applied for the data having DFS values larger than 0.6 for CH_4. TIR data (L2 Version 0.10) were only available from 16 March to 24 November 2010 from the GOSAT User Interface Gateway at the time the analysis has been performed. These retrievals provide vertical profiles of mixing ratio of CH_4 from 1000 to 100 hPa. Comparisons with aircraft measurements during flights between Tokyo Narita airport in Japan and Guam airport (13° N, 144° E) show that the average difference between the GOSAT (TIR) and aircraft CH_4 values (TIR – aircraft) is −5 ppbv, and the 1σ standard deviation is 15 ppbv (Saitoh et al., 2012). Daily maritime profiles of CH_4 have been averaged in $1^\circ \times 1^\circ$ bins over the MB.

ACPD
14, 9975–10024, 2014

2.2 The model data

2.2.1 The MOCAGE data

MOCAGE (MOdèle de Chimie Atmosphérique à Grande Echelle) (Peuch et al., 1999) is a 3-D CTM which covers the planetary boundary layer, the free troposphere, and the stratosphere. It provides a number of optional configurations with varying domain geometries and resolutions, as well as chemical and physical parameterization packages. It has the flexibility to use several chemical schemes for stratospheric and tropospheric studies. MOCAGE is used for applications such as: operational chemical weather forecasting in Météo-France (Dufour et al., 2004); tropospheric and stratospheric research studies (e.g., Claeyman et al., 2010; Ricaud et al., 2009); and data assimilation research (e.g., El Amraoui et al., 2010; Claeyman et al., 2011). In this study, MOCAGE is forced dynamically by wind and temperature fields from the analyses of the ARPEGE model, the global operational weather prediction model of Météo-France (Courtier et al., 1991). The MOCAGE horizontal resolution used for this study is $2^\circ \times 2^\circ$ and the model uses a semi-Lagrangian transport scheme. It includes 47 hybrid (sigma, P) levels from the surface up to 5 hPa, where sigma $= P/P_s$; P and P_s are the pressure and the surface pressure, respectively. The vertical resolution of MOCAGE is about 800 m around the tropopause, 400–800 m in the troposphere and 40–400 m in the 7 levels of the boundary layer. Chemistry used within MOCAGE is a combination of tropospheric (RACM described in Stockwell et al., 1997) and stratospheric (REPROBUS described in Lefèvre et al., 1994) chemical schemes. Initial chemical conditions are taken from climatological fields over a spin-up period of 3 months allowing the model to quickly bring chemical fields to realistic spatial distributions. Surface emissions prescribed in MOCAGE are based upon yearly- or monthly-averaged climatologies. More precisely, the CH_4 surface emissions are split into anthropogenic sources taken from the Intergovernmental Panel on Climate Change (IPCC) (Dentener et al., 2005), biomass burning (van de Werf et al., 2003) and biogenic sources (Michou and Peuch, 2002). The CH_4 climatologies are representative of year 2000 for a to-

ACPD
14, 9975–10024, 2014

tal emission rate of 534 Tg(CH_4) yr^{-1}. For more information on surface emissions, the reader should refer to Dentener et al. (2005).

2.2.2 The CNRM-AOCCM data

The atmospheric model embedded in CNRM-AOCCM is presented in Huszar et al. (2013) based on the Atmosphere-Ocean General Circulation Model (AOGCM) CNRM-CM5 described in Voldoire et al. (2013). The main difference between CNRM-CM5 and CNRM-AOCCM resides in the "online" coupling with a stratospheric chemistry which is based on the REPROBUS scheme. This scheme is applied on the whole vertical column, except between the surface and the 560 hPa level where long-lived chemical species are relaxed towards global average surface value following the A1B scenario from IPCC (2007). The A1B scenario mainly describes a future world of very rapid economic growth, global population that peaks in mid-century and declines thereafter, and the rapid introduction of new and more efficient technologies. Convection of species is not considered. In this chemistry version, the 3-D distribution of the seven absorbing gases (H_2O, CO_2, O_3, CH_4, N_2O, CFC11, and CFC12) is then provided by the chemistry module of CNRM-AOCCM and interacts with the radiative calculations. More details can be found in Michou et al. (2011). In the CNRM-CM default version, there are only 31 vertical levels of which 5 are in the stratosphere. For stratospheric chemistry studies, the number of vertical levels has been increased to 60 layers (26 of them being in the stratosphere). This increase of vertical resolution requires to reduce the time-step from 30 to 15 min. Additionally, as there are about 50 3-D supplementary species, the horizontal resolution was reduced from 1.4° to 2.8° to reduce computational costs. As a consequence of the resolution decrease, the horizontal diffusion and gravity wave drag have been adjusted. Distribution of atmospheric constituents at the surface are zonally symmetric below 500 hPa (see Fig. 12) and greenhouse gases follow the A1B scenario on atmospheric chemistry and climate for the period of 1940–

ACPD
14, 9975–10024, 2014

2100. In the present analysis, for this model, we only consider the climatological period 2001–2010.

2.2.3 The LMDz-OR-INCA data

The INteraction between Chemistry and Aerosol (INCA) model is used to simulate the distribution of aerosols and gaseous reactive species in the troposphere. INCA computes primary emissions, deposition and chemical equations with a time-step of 30 min. In the present configuration, the model includes 19 hybrid vertical levels extending up to 4 hPa, and a horizontal resolution of 1.9° in latitude and 3.75° in longitude. INCA is coupled online to the LMDz General Circulation Model (GCM) to account, with different degrees of complexity, for climate chemistry interactions. In the simulations described here, LMDz is coupled with the ORCHIDEE (Organizing Carbon and Hydrology in Dynamic Ecosystems) dynamic global vegetation model (Krinner et al., 2005) for soil/atmosphere exchanges of water and energy (Hourdin et al., 2006), but not for biogenic CO_2 or Volatile Organic Compounds (VOCs) fluxes. Together, these three models form the LMDz-OR-INCA model. Fundamentals for the gas phase chemistry are presented in Hauglustaine et al. (2004) and first results with the full tropospheric gaseous chemical scheme are presented by Folberth et al. (2006). The model includes 223 homogeneous chemical reactions, 43 photolytic reactions and 6 heterogeneous reactions including non-methane hydrocarbon oxidation pathways and aerosol formation. The LMDz-OR-INCA simulation covers four future projections of emissions for the 2000–2100 period. The Representative Concentration Pathways (RCP) emissions are used (Lamarque et al., 2011). They correspond to emission trajectories compatible with the evolution of radiative forcing equivalent in 2100 to 2.6, 4.5, 6.0 and 8.5 $W m^{-2}$ relative to pre-industrial values (we label in the manuscript RCP 2.6, 4.5, 6.0 and 8.5). These scenarios are intended to span a range of climate forcing levels (Moss et al., 2010). In the present analysis, for this model, we only consider the climatological period 2001–2010.

ACPD
14, 9975–10024, 2014

3 Meteorology and climatology

Figure 1 shows the CH_4 fields calculated by MOCAGE for summer (June-July-August, JJA) 2009 over the MB at 850, 500 and 200 hPa, superimposed with the associated wind fields from the ARPEGE analyses averaged over the same period. The vertical distribution of CH_4 as calculated by MOCAGE in summer 2009 along an east–west axis above the MB is presented on Fig. 2. The vertical distributions of CH_4 calculated by MOCAGE for summer 2009 along a north–south axis at three different longitudes, namely at 7° E, 19° E and 29° E, are displayed on Fig. 3. As for Figs. 1–3, the CH_4 fields as calculated by MOCAGE for winter (December-January-February, DJF) 2009 over the MB are presented on Figs. 4–6 at 850, 500 and 200 hPa, along an east–west axis, and along a north–south axis at three different longitudes, namely at 7° E, 19° E and 29° E, respectively. On Figs. 2, 3, 5 and 6, the MOCAGE CH_4 fields are superimposed with the associated wind fields from ARPEGE analyses and the cold point tropopause from the NOAA/NCEP reanalyses.

Considering the meteorology of the MB, we observe two different regimes. (1) In winter, and more generally from autumn to spring (not shown), from the boundary layer to the upper troposphere, air masses are essentially coming from either Europe or Eastern Atlantic Ocean. (2) In summer, the meteorology of EMB and WMB is affected by different processes. In the planetary boundary layer, cells develop in the WMB, and air masses come from Europe, Northern Africa and Eastern Atlantic Ocean, whilst in the EMB, air masses are originated from four major source regions: (i) long fetch of maritime European air masses from north-west throughout the whole year, (ii) North east continental flow originating in south Eastern Europe (Etesian winds) in summer, (iii) South-east flow from the Arabian Peninsula occurring in the fall, and (iv) South-west flow along the North-African coast most frequent during late winter and spring (Dayan, 1986). In the middle troposphere, air masses are essentially coming from the west for both parts of the basin. In the upper troposphere, in the WMB, air masses are essentially coming from the west, but in the EMB, air masses are also originated from

ACPD
14, 9975–10024, 2014

Northern Africa and the Arabic Peninsula (Ziv et al., 2004; Liu et al., 2009), and even farther away, from Asia (we will discuss this point in Sects. 4 and 5). Note that the EMB and WMB are also affected by the location of the descending branch of the Hadley cell (Figs. 3 and 6). All these summer climatologies are consistent with the detailed works presented in e.g. Millán et al. (1997), Lelieveld et al. (2002), Ziv et al. (2004) and Schicker et al. (2010).

Seasonally-averaged wind fields from ARPEGE analyses show that there are two regimes in the surface pressure values which could be separated into winter and summer periods. During the summer in the WMB, there is a higher pressure regime than in the EMB. In the lowermost troposphere (850 hPa), an anticyclonic cell develops in the WMB that has an impact on the distribution of CH_4 by producing a local minimum (Fig. 1). At 850 hPa, air masses are coming from Europe, North Africa and the Atlantic Ocean. In the mid-troposphere (500 hPa), air masses are coming from Europe, and the Atlantic Ocean; and a pronounced east–west gradient is detected with more CH_4 on the EMB. In the upper troposphere (200 hPa), air masses are originated from the Atlantic Ocean (even North America) and from Asia producing over the MB an obvious north–south gradient with more CH_4 in the South (upper troposphere) than in the North (lower stratosphere). Because the temperature of the Mediterranean Sea is smaller than on the surrounding continents, a systematic subsidence is present (Fig. 3) whatever the longitudinal bin considered. The Hadley cell is further displaced over the Northern Africa (Fig. 3) and its downward branch in the area 30–35° N produces a systematic descent in the EMB. The tropopause moves up from ~ 200 hPa in the WMB to ~ 175 hPa in the EMB.

In winter, the meteorological state of the MB is much more homogeneous with westerlies blowing whatever the pressure considered from 850 to 200 hPa (Figs. 4 and 5). North–south (and to a lesser extent east–west) gradients can also be detected associated to the local sources of emission over Europe at 850 hPa and to the stratosphere/troposphere transition at 200 hPa. Contrarily to summer, since the temperature of the Mediterranean Sea is greater than that of the surrounding continents, a system-

ACPD
14, 9975–10024, 2014

atic upward motion is present (Fig. 6) whatever the longitudinal bin considered. The Hadley cell is further displaced to the South (latitude < 30° N) and its downward branch does not affect significantly the EMB. The tropopause pressure is rather stable from the WMB to the EMB, around 260 hPa.

4 CH_4 variability

4.1 Global distribution

Figure 7 shows the distributions of CH_4 total columns as measured by IASI over the MB averaged in summer 2009, together with the MOCAGE results in time coincidence. Also shown are the distributions of the CH_4 mixing ratios as measured by AIRS at 260 hPa over the MB averaged in summer 2009, together with the MOCAGE results at 200 hPa in time coincidence. Only the maritime pixels are considered in this figure. The measured and modelled data are selected within the boxes (36–45° N, 1–12° E) and (30–37° N, 26–37° E) to represent the WMB and the EMB (blue squares in each figure), respectively.

Although considered as a well-mixed species in the troposphere, the CH_4 spatial distribution over the MB in the middle troposphere (inferred from the sensitivity of the CH_4 total columns from IASI) and in the upper troposphere (200–260 hPa) shows some gradients (~ 60 ppbv or ~ 4 %) in total column mixing ratios and (~ 30–150 ppbv or ~ 2–9 %) in mixing ratios at 200–260 hPa in summer (JJA) 2009 between the WMB and the EMB, but also between the Northern and the Southern parts of the MB (although not detected in the IASI data set). In the mid-to-upper troposphere, these east–west gradients are not originated from the sources of CH_4 that are more intense in Europe than in Northern Africa or in Middle Asia (Fig. 1) but rather from the long-range transport of Asian-origin air masses and the subsidence of air masses in the EMB (see Figs. 1–3 and detailed discussion in Sect. 5).

ACPD
14, 9975–10024, 2014

Quantitatively, there is a positive bias in MOCAGE vs. IASI of less than 30 ppbv (2 %) in CH_4 total column mixing ratio. The east–west gradient is rather consistent between IASI and MOCAGE but the north–south modelled gradient is not detected in the IASI data set. In the upper troposphere (200–260 hPa), MOCAGE and AIRS CH_4 mixing ratios are very consistent with gradients more accentuated in the model (∼ 150 ppbv) than in the AIRS data sets (∼ 30 ppbv). A systematic negative bias of MOCAGE compared to AIRS of ∼ 100 ppbv up to 150 ppbv (10 %) in the Northern MB is detected. We discuss in the next section the consistency of the vertical profiles of CH_4 as measured by the different spaceborne sensors and as calculated by MOCAGE together with the associated biases.

4.2 Vertical profiles

Figure 8 shows the vertical profiles of CH_4 as measured by AIRS (750–100 hPa) and GOSAT (1000–100 hPa) and as calculated by MOCAGE (1000–100 hPa) averaged over the EMB and the WMB depending on the four seasons: winter (DJF), spring (March-April-May, MAM), summer (JJA) and autumn (September-October-November, SON) 2010. There is a good agreement to within 20–30 ppbv between AIRS and GOSAT data in the vertical domain 750–200 hPa. GOSAT is systematically greater than AIRS by about 20–30 ppbv for pressure greater than 300 hPa, whilst, for pressure less than 300 hPa, AIRS is systematically greater than GOSAT by 20 ppbv degrading to 50–200 ppbv at 100 hPa. But the shape of the vertical spaceborne profiles is consistent between AIRS and GOSAT. Separately, whatever the season considered, the MOCAGE vertical profiles systematically show a maximum at 300 hPa that is not present in any of the spaceborne measurements and a strong decrease above.

In order to assess the impact of the vertical sensitivity of the spaceborne measurements to the CH_4 profiles, we have applied the AIRS averaging kernels issued from the AIRS retrieval method (Susskind et al., 2011) and provided by NASA for each AIRS pixel to the profiles calculated by MOCAGE. Note that the AIRS a priori vertical profiles are not used in our study since we are only interested in the vertical shape of the CH_4

ACPD
14, 9975–10024, 2014

profile and not the absolute amount of CH_4. Degrading the vertical resolution of the MOCAGE profiles by the convolution of averaging kernels (Fig. 8) does show a strong impact on the vertical shape of the CH_4 profiles since the strong maximum at 300 hPa is no longer present. Convolved MOCAGE CH_4 profiles are now very consistent with AIRS CH_4 profiles whatever the season considered. The systematic bias of ~ 100 ppbv between AIRS and MOCAGE convolved profiles is related to the fact that no a priori information contributes to the convolved profile. Along the vertical, it is almost impossible to validate the spaceborne profiles with an external data set since, even within the Total Carbon Column Observing Network (http://www.tccon.caltech.edu/) giving accurate and precise column-averaged abundances of atmospheric constituents including CH_4 (Wunch et al., 2010) because no measurement sites are unfortunately available in the vicinity of the MB.

Near the surface, the amount of CH_4 is about 1 800–1 850 ppbv for MOCAGE, and is on average less than the CH_4 GOSAT data by about 20–80 ppbv. At this stage, it is worthwhile considering surface data within the MB. The NOAA Earth System Research Laboratory (ESRL) In Situ Methane Measurements provide some surface CH_4 measurements within and/or in the vicinity of the MB: Lampedusa, Italy (35.52° N, 12.62° E, 45 a.m.s.l.), Centro de Investigacoin de la Baja Atmosfera (CIBA), Spain (41.81° N, 4.93° W, 845 a.m.s.l.) and Negev Desert, Israel (30.86° N, 34.78° E, 477 a.m.s.l.). On average, these three sites show a surface CH_4 annual mean of about 1 875 ppbv in 2010, with an annual oscillation of ~ 20 ppbv amplitude. Consequently, the amount of surface CH_4 in the MOCAGE run for 2010 is actually slightly low biased by about 20–30 ppbv (1 %). This is consistent with the MOCAGE CH_4 climatologies from the year 2000 used to initiate the runs, knowing that the surface CH_4 amounts measured at Negev Desert increased from ~ 1850 to ~ 1875 ppbv from 2000 to 2010 (not shown). The slight differences between the EMB and the WMB according to the season and height are studied in detail in the next section.

ACPD
14, 9975–10024, 2014

4.3 Seasonal variations of the east–west difference

The seasonal variation of the differences in CH_4 fields between the EMB and the WMB (we label now as "E–W") as measured by AIRS, GOSAT and IASI and as calculated by LMDz-OR-INCA, CNRM-AOCCM and MOCAGE is presented in Fig. 9 when considering the upper troposphere (AIRS, GOSAT, LMDz-OR-INCA and CNRM-AOCCM at 260 and 300 hPa) and the middle troposphere (IASI and MOCAGE total column mixing ratios). In the middle and upper troposphere (Fig. 9), the modelled and measured seasonal variation of E–W is rather consistent to each other showing a maximum (peak) in summer and a wide minimum in winter.

If we consider the time evolution of the total column mixing ratios (namely focussing on the middle troposphere), we can note that both MOCAGE and IASI show a maximum in summer, although 3 times greater in MOCAGE ($\sim$ 60 ppbv) than in IASI ($\sim$ 20 ppbv) in July and August. The minimum in January–February is close to zero but slightly positive in October (5–10 ppbv). The much stronger maximum in August calculated by MOCAGE compared to IASI CH_4 total columns might be attributable to the sensitivity of spaceborne measurements in the middle troposphere whilst the MOCAGE tropospheric columns cover the entire troposphere from the surface to the top of the model atmosphere, namely 5 hPa.

In the upper troposphere (300 hPa), the spaceborne instrument datasets show a E–W maximum in summer of $\sim$ 12 ppbv in August for AIRS and a E–W wide maximum of $\sim$ 5 ppbv in July–September for GOSAT. A E–W peak of $\sim$ 10 ppbv in July–August is also calculated by CNRM-AOCCM although, in the LMDz-OR-INCA dataset, the E–W maximum is slightly positive in August ($\sim$ 2 ppbv). The minimum in the satellite datasets is observed in March–April and is negative (from –15 to –20 ppbv) consistently with the LMDz-OR-INCA dataset whilst the CNRM-AOCCM E–W minimum is less intense (–6 ppbv in February and April). The peak-to-peak amplitude of the E–W seasonal variation is consistent within all the data sets: $\sim$ 25 ppbv for the measurements and slightly less for the models, $\sim$ 15 ppbv. This represents a $\sim$ 1.5 % variation of CH_4 in the

ACPD
14, 9975–10024, 2014

E–W over the entire year. Considering the average number of observations used per month to calculate the E–W variation, namely ∼ 40 000 for IASI, the monthly random error attributed to the E–W IASI CH_4 is about 0.1 %, much less than the observed peak-to-peak yearly variation. We estimate that the AIRS monthly random error attributed to the E–W CH_4 is comparable to the one calculated for IASI, but the GOSAT monthly random error should be greater than the ones calculated for AIRS and IASI by a factor 2 to 4 due to the smaller number of observations used in the analysis. We discuss in the next section the origin of the summer peak in the E–W seasonal variation.

5 Discussions

Based on the CNRM-AOCCM and LMDz-OR-INCA model results over the climatological period 2001–2010, we consider (Fig. 10) the E–W CH_4 seasonal evolution at pressure levels from the lowermost troposphere to the lowermost stratosphere (850, 700, 500, 300, 200 and 100 hPa) and different scenarios for LMDz-OR-INCA (RCPs 2.6, 4.5, 6.0 and 8.5). The two models behave distinctively in the entire troposphere, and agree very well in the lowermost stratosphere. In the lower troposphere (850 and 700 hPa), the E–W CH_4 seasonal evolution from LMDz-OR-INCA exhibits a strong semi-annual oscillation of ±10–15 ppbv peaking in winter and summer for the 4 RCPs whilst the evolution from the CNRM-AOCCM shows a weak annual oscillation of 4–5 ppbv amplitude, with a strong minimum in summer, namely out-of-phase relative to the LMDz-OR-INCA variation. In the middle troposphere at 500 hPa, the 4 LMDz-OR-INCA outputs exhibit a net maximum in August of ∼ 8 ppbv with minima ranging from −2 to −12 ppbv from October to June, whilst the output from CNRM-AOCCM again shows a strong minimum in summer of about −4 ppbv. At this stage, it is important to recall that the two models are Global Circulation Models (GCMs) with an on-line chemistry. The emissions of CH_4 are time-, longitude- and latitude-dependent in LMDz-OR-INCA. In CNRM-AOCCM, there is no emission of CH_4 but mixing ratios of CH_4 between the surface and the 560 hPa level are relaxed towards evolving global mean surface abundances.

ACPD
14, 9975–10024, 2014

This explains why the two models behave separately for pressures greater or equal to 500 hPa. Note that, regarding the shape of the E–W CH_4 seasonal evolution, there is no significant difference within the different scenarios of the LMDz-OR-INCA outputs. But only the RCP 4.5 scenario gives systematically a positive summer peak in the E–W CH_4 seasonal evolution whatever the pressure level considered consistently with the measurements.

In the upper troposphere (200 and 300 hPa), the outputs from the two models show a peak in summer in the E–W CH_4 seasonal evolution, but this differs from the RCPs considered for LMDz-OR-INCA. The maximum is much more intense in CNRM-AOCCM (~ 8 ppbv in July–August and ~ 30 ppbv in June–July at 300 and 200 hPa, respectively) than in LMDz-OR-INCA (~ 1 and ~ 10 ppbv in August for RCP 4.5 but only –4 and +4 ppbv in August for RCP 8.5 at 300 and 200 hPa, respectively; one peak at –4 ppbv in August for RCP 6.0 at 300 hPa but no peak at 200 hPa; no peak for RCP 2.6 neither at 300 nor at 200 hPa). In the lower stratosphere (100 hPa), all the model outputs are consistent to each other showing an annual oscillation, with a wide maximum in summer (60–80 ppbv) and a wide minimum in winter (20–35 ppbv). On average, from 500 to 200 hPa, only the RCP 4.5 scenario from LMDz-OR-INCA shows a positive maximum in summer but always much less intense than the CNRM-AOCCM values (for 300 and 200 hPa). We can note that the summer peak in E–W seasonal evolution has also been observed and calculated by considering other constituents like CO and O_3 (not shown) from the middle to the upper troposphere. This is the main issue of a forthcoming paper.

As stated in Sect. 3, interpreting the temporal evolution of the E–W CH_4 seasonal evolution along the vertical also requires to consider the evolution of CH_4 over the Asian continent because of the importance of long-range transport. We represent the fields of CH_4 as calculated by CNRM-AOCCM and by LMDz-OR-INCA (4 scenarios) at 200 hPa in summer averaged over the climatological period 2001–2010 over a wide area covering the MB and the Asian continent in Fig. 11, whilst the CH_4 fields specified and/or calculated in the lowermost level (surface level) are shown in Fig. 12.

ACPD
14, 9975–10024, 2014

Numerous studies have already evaluated the impact of transport vs. emission of pollutants and aerosols over the MB and its temporal variability considering different pollutants, chemical compounds and aerosols (see e.g. Wanger et al., 2000; Lelieveld et al., 2002; Pfister et al., 2004; Kallos et al., 2007). As stated in Sect. 3, two main dynamic factors affect the EMB: (1) the upper to mid-tropospheric subsidence, and (2) the lower-level cool Etesian winds (Ziv et al., 2004). Although the EMB is characterized by strong descent in the middle and upper troposphere in summer, transport from the boundary layer accounts for about 25 % of the local Middle Eastern contribution to the ozone enhancement in the middle troposphere (Liu et al., 2009). Elevated CO episodes in EMB during summer can also be attributed to synoptic conditions prone to favorable transport from Turkey and Eastern Europe towards the EMB rather than increased emissions (Drori et al., 2012). Dust reaching the EMB can be differentiated either from the west and southwest (i.e. the Sahara) or from east of the Negev (i.e. from Arabia) (Dayan et al., 1991).

From Rodwell and Hoskins (1996), it is known that there is a meteorological link between monsoons and the dynamics of the deserts and more precisely between the Asian monsoon and the EMB summer regime. The subsidence centre over the EMB owes its location, timing of onset and intensity to the Asian monsoon, and not to the Hadley circulation. Although it takes less than one day to reach the upper troposphere within the Asian monsoon, back-trajectory calculation (Ziv et al., 2004) shows that it takes about 3–4 days for an air parcel to reach and descent the upper tropospheric EMB from the vicinity of the anticyclone that develops over the Asian monsoon. Inside the Asian monsoon anticyclone (AMA), pollutants like CO originating from the surface constitute about 50 % of the CO concentration at 100 hPa (Park et al., 2009), with the reminder resulting from chemical production in the troposphere. Most of the CO within the AMA comes from India and South East Asia, with an insignificant contribution from the Tibetan Plateau.

In our study, whatever the amount of CH_4 at the surface and its horizontal distribution, 1850–2000 ppbv for LMDz-OR-INCA consistently with the emission sources

ACPD
14, 9975–10024, 2014

(Asia, Northern and Eastern Europe, Central Africa) or 1820 ppbv uniformly spread for CNRM-AOCCM (Fig. 12), the Asian monsoon traps elevated amounts of CH_4 that converge through the depression, and are uplifted up to the upper troposphere at 200 hPa (Fig. 11). At this level, the AMA re-distributes elevated amounts of CH_4 towards Middle East, North Africa and the EMB. This phenomenon has been studied and analyzed in detail over Asia by considering various parameters: dynamical parameters (potential vorticity) and chemical species (H_2O, CO and O_3) as in e.g. Randel and Park (2006); Park et al. (2009).

The horizontal distribution of CH_4 calculated by the two models at 200 hPa drastically differs but the local maxima are all centred within the AMA. A zonally-symmetric structure showing a strong South–North gradient in CH_4 is modelled by CNRM-AOCCM with maxima in the tropics (1850 ppbv) and minima at high latitudes (1740 ppbv) and a local maximum centred within the core of the AMA with values greater than 1860 ppbv elongated towards two axis: (1) South-East Asia and (2) Middle East and EMB. The CH_4 field calculated by LMDz-OR-INCA considering the 4 scenarios also shows a primary maximum over Northern India and a secondary maximum over North-East Asia but the horizontal distribution is not zonally-symmetric due to a non-zonally-symmetric CH_4 surface field. As expected, the CH_4 maxima within the AMA range from 1710 to 1750 ppbv with increasing RCPs from 2.6 to 8.5. In all the scenarios considered, an elongated tongue of enriched CH_4 enters the EMB. In conclusion, the systematic summer maximum observed and calculated in the E–W CH_4 seasonal evolution from the middle to upper troposphere is induced by the impact of the AMA that re-distributes pollutants (including CH_4) trapped by the Asian monsoon to the EMB. In the lower troposphere, the local sources of emission in the vicinity of the MB mainly affect the E–W CH_4 seasonal evolution.

ACPD
14, 9975–10024, 2014

6 Conclusions

The present study is part of the Chemical and Aerosol Mediterranean Experiment (ChArMEx) programme. It intends to study the tropospheric CH_4 time and space variations above the Mediterranean Basin (MB) to (1) assess the variability and (2) attribute the variability to different processes at both meso and global scales depending on the season and the altitude layer considered. The datasets we used is twofold. (1) The spaceborne measurements from Thermal Infrared (TIR) instruments: Thermal And Near infrared Sensor for carbon Observations - Fourier Transform Spectrometer (TANSO-FTS) instrument on the Greenhouse gases Observing SATellite (GOSAT) satellite, the Atmospheric InfraRed Spectrometer (AIRS) on the Aura platform and the Infrared Atmospheric Sounder Interferometer (IASI) instrument aboard the MetOp-A platform. (2) The model results from the Chemical Transport Model (CTM) MOCAGE, and the two Chemical Climate Models (CCMs) CNRM-AOCCM and LMDz-OR-INCA (the later considering different emission scenarios, RCPs 2.6, 4.5, 6.0 and 8.5). The period under interest spans from 2008 to 2011 in the case of the satellite measurements and the MOCAGE model results whilst, regarding the CCMs, we have averaged the model outputs over the climatological period from 2001 to 2010.

We have only considered the pixels measured over the Mediterranean Sea in order to minimize the systematic biaises among pixels (day vs. night, continent vs. maritime). Maritime pixels are the least contaminated pixels with surface emissivity which, on the land, could have important impact on a retrieved value. Also the diurnal variation of surface temperature has an amplitude that is less intense over the sea than over the continent, that is to say the sensitivity of the IR measurements over the sea during day and night is somewhat consistent and concentrated in the mid-troposphere although the sensitivity of land IR nadir measurements is, on average, lower during the day than during the night depending on the thermal contrast at the surface.

Although CH_4 has a lifetime of 12 years in the troposphere and is supposed to be well mixed, an east–west gradient in CH_4 is observed and modelled whatever the season

ACPD
14, 9975–10024, 2014

considered from the middle to the upper troposphere. In winter, air masses mainly originating from Atlantic Ocean and Europe tend to favour an elevated amount of mid-to-upper tropospheric CH_4 in the West compared to the East of the MB, with a general upward transport above the MB. In summer, the meteorological state of the MB is changed, favouring air from Northern Africa and Middle East together with Atlantic Ocean and Europe, with a general descent above the Eastern MB. The Asian monsoon traps and uplifts high amounts of CH_4 to the upper troposphere. It is shown that the Asia monsoon Anticyclone redistributes pollutants (namely CH_4) towards North Africa and Middle East to finally reach and descent in the Eastern bank of the MB. Consequently, the mid-to-upper tropospheric CH_4 is much greater in the East than in the West of the MB.

The seasonal variation of the difference in CH_4 between the East and the West MB shows a maximum in summer for pressures from 500 to 100 hPa considering both spaceborne measurements and model results whatever the emission scenarios used for the CCMs. But only the RCP 4.5 scenario gives systematically a positive summer peak whatever the pressure level considered, consistently with the measurements. From this study, we can conclude that CH_4 in the mid-to-upper troposphere over the MB is mainly affected by long-range transport, particularly intense in summer from Asia. In the low-to-mid troposphere, the local sources of emission in the vicinity of the MB mainly affect the CH_4 variability. Other constituents are also affected by this summer mechanism e.g. O_3 and CO (not shown). In a forthcoming paper, the time evolution of the CH_4, O_3 and CO fields above the MB and at the Asian scale is being studied by considering the outputs from different CCMs in the contemporary period (2000–2010) in order to study the future evolution of the chemical climate over the MB by 2100.

Acknowledgements. We would like to thank the following institutes and programme for funding our study: Centre National de la Recherche Scientifique-Institut National des Sciences de l'Univers/CNRS-INSU, Centre National des Etudes Spatiales/CNES, Agence de l'Environnement et de la Maîtrise del'Energie/ADEME through the programme the Mediterranean Integrated STudies at Regional And Local Scales/MISTRALS Chemistry-Aerosol Mediterranean Experiment/ChArMEx. We also thank the following data bases for accessing

ACPD
14, 9975–10024, 2014

the data: the French database Ether, the European Organisation for the Exploitation of Meteorological Satellites, the GOSAT User Interface Gateway, the National Oceanic and Atmospheric Administration, the British Atmospheric Data Centre to access the LMDz-OR-INCA model data through the international Atmospheric Chemistry and Climate Model Intercomparison Project initiative, and the Global Atmosphere Watch from the World Meteorological Organization.

References

August, T., Klaes, D., Schlüssel, P., Hultberg, T., Crapeau, M., Arriaga, A., O'Carroll, A., Coppens, D., Munro, R., and Calbet, X.: IASI on Metop-A: operational level 2 retrievals after five years in orbit, J. Quant. Spectrosc. Ra., 113, 11, 1340–1371, 2012.

Aumann, H., Chahine, T., Gautier, C., Goldberg, D., Kalnay, E., McMillin, M., Revercomb, H., Rosenkranz, W., Smith, L., Staelin, H., Strow, L., and Susskind, J.: AIRS/AMSU/HSB on the aqua mission: design, science objectives, data products, and processing systems, IEEE T. Geosci. Remote, 41, 253–264, doi:10.1109/TGRS.2002.808356, 2003.

Bergamaschi, P., Frankenberg, C., Fokke Meirink, J., Krol, M., Villani, M. G., Houweling, S., Dentener, F., Dlugokencky, E. J., Miller, J. B., Gatti, L. V., Engel, A., and Levin, I.: Inverse modeling of global and regional CH_4 emissions using SCIAMACHY satellite retrievals, J. Geophys. Res., 114, D22301, doi:10.1029/2009JD012287, 2009.

Betchold, P., Bazile, E., Guichard, F., Mascart, P., and Richard, E.: A mass flux convection scheme for regional and global models, Q. J. Roy. Meteor. Soc., 127, 869–886, 2001.

Bousquet, P., Ringeval, B., Pison, I., Dlugokencky, E. J., Brunke, E.-G., Carouge, C., Chevallier, F., Fortems-Cheiney, A., Frankenberg, C., Hauglustaine, D. A., Krummel, P. B., Langenfelds, R. L., Ramonet, M., Schmidt, M., Steele, L. P., Szopa, S., Yver, C., Viovy, N., and Ciais, P.: Source attribution of the changes in atmospheric methane for 2006–2008, Atmos. Chem. Phys., 11, 3689–3700, doi:10.5194/acp-11-3689-2011, 2011.

Buchwitz, M., Rozanov, V. V., and Burrows, J. P.: A near-infrared optimized DOAS method for the fast global retrieval of atmospheric CH_4, CO, CO_2, H_2O, and N_2O total column amounts from SCIAMACHY Envisat-1 nadir radiances, J. Geophys. Res., 105, 15231–15245, doi:10.1029/2000JD900191, 2000.

Claeyman, M., Attié, J.-L., El Amraoui, L., Cariolle, D., Peuch, V.-H., Teyssèdre, H., Josse, B., Ricaud, P., Massart, S., Piacentini, A., Cammas, J.-P., Livesey, N. J., Pumphrey, H. C., and

ACPD
14, 9975–10024, 2014

Edwards, D. P.: A linear CO chemistry parameterization in a chemistry-transport model: evaluation and application to data assimilation, Atmos. Chem. Phys., 10, 6097–6115, doi:10.5194/acp-10-6097-2010, 2010.

Claeyman, M., Attié, J.-L., Peuch, V.-H., El Amraoui, L., Lahoz, W. A., Josse, B., Ricaud, P., von Clarmann, T., Höpfner, M., Orphal, J., Flaud, J.-M., Edwards, D. P., Chance, K., Liu, X., Pasternak, F., and Cantié, R.: A geostationary thermal infrared sensor to monitor the lowermost troposphere: O_3 and CO retrieval studies, Atmos. Meas. Tech., 4, 297–317, doi:10.5194/amt-4-297-2011, 2011.

Clerbaux, C., Chazette, P., Hadji-Lazaro, J., Mégie, G., Müller, J.-F., and Clough, S. A.: Remote sensing of CO, CH_4, and O_3 using a spaceborne nadir-viewing interferometer, J. Geophys. Res., 103, 18999–19013, doi:10.1029/98JD01422, 1998.

Courtier, P., Freydier, C., Geleyn, J. F., Rabier, F., and Rochas, M.: The ARPEGE project at METEO-FRANCE, in: Proc ECMWF Workshop, Numerical methods in atmospheric modelling, 9–13 September 1991, 2, 193–231, ECMWF, Shinfield Park, Reading, UK, 1991.

Crevoisier, C., Nobileau, D., Fiore, A. M., Armante, R., Chédin, A., and Scott, N. A.: Tropospheric methane in the tropics – first year from IASI hyperspectral infrared observations, Atmos. Chem. Phys., 9, 6337–6350, doi:10.5194/acp-9-6337-2009, 2009.

Crevoisier, C., Nobileau, D., Armante, R., Crépeau, L., Machida, T., Sawa, Y., Matsueda, H., Schuck, T., Thonat, T., Pernin, J., Scott, N. A., and Chédin, A.: The 2007–2011 evolution of tropical methane in the mid-troposphere as seen from space by MetOp-A/IASI, Atmos. Chem. Phys., 13, 4279–4289, doi:10.5194/acp-13-4279-2013, 2013.

Crisp, D., Atlas, R. M., Bréon, F.-M., Brown, L. R., Burrows, J. P., Ciais, P., Connor, B. J., Doney, S. C., Fung, I. Y., and Jacob, D. J.: The Orbiting Carbon Observatory (OCO) mission, Adv. Space Res., 34, 700–709, 2004.

Dayan, U.: Climatology of back trajectories from Israel based on synoptic analysis, J. Clim. Appl. Meteorol., 25, 591–595, doi:10.1175/1520-0450(1986)025<0591:COBTFI>2.0.CO;2, 1986.

Dayan, U. and Levy, I.: Relationship between synoptic-scale atmospheric circulation and ozone concentrations over Israel, J. Geophys. Res., 107, 4813, doi:10.1029/2002JD002147, 2002.

Dayan, U., Heffter, J., Miller, J., and Gutman, G.: Dust Intrusion Events into the Mediterranean Basin, J. Appl. Meteorol., 30, 1185–1199, 1991.

Dayan, U., Ziv, B., Shoop, T., and Enzel, Y.: Suspended dust over south-eastern Mediterranean and its relation to atmospheric circulations, Int. J. Climatol., 28, 915–924, 2007.

ACPD
14, 9975–10024, 2014

Dentener, F., Stevenson, D., Cofala, J., Mechler, R., Amann, M., Bergamaschi, P., Raes, F., and Derwent, R.: The impact of air pollutant and methane emission controls on tropospheric ozone and radiative forcing: CTM calculations for the period 1990-2030, Atmos. Chem. Phys., 5, 1731–1755, doi:10.5194/acp-5-1731-2005, 2005.

Drori, R., Dayan, U., Edwards, D. P., Emmons, L. K., and Erlick, C.: Attributing and quantifying carbon monoxide sources affecting the Eastern Mediterranean: a combined satellite, modelling, and synoptic analysis study, Atmos. Chem. Phys., 12, 1067–1082, doi:10.5194/acp-12-1067-2012, 2012.

Dufour, A., Amodei, M., Ancellet, G., and Peuch, V.-H.: Observed and modelled "chemical weather" during ESCOMPTE, Atmos. Res., 74, 161–189, 2005.

El Amraoui, L., Attié, J.-L., Semane, N., Claeyman, M., Peuch, V.-H., Warner, J., Ricaud, P., Cammas, J.-P., Piacentini, A., Josse, B., Cariolle, D., Massart, S., and Bencherif, H.: Midlatitude stratosphere – troposphere exchange as diagnosed by MLS O_3 and MOPITT CO assimilated fields, Atmos. Chem. Phys., 10, 2175–2194, doi:10.5194/acp-10-2175-2010, 2010.

Erel, Y., Kalderon-Asael, B., Dayan, U., and Sandler, A.: European pollution imported by cooler air masses to the eastern Mediterranean during the summer, Environ. Sci. Technol., 41, 5198–5203, 2007.

EUMETSAT: IASI Level 2 Products Guide, EUM/OPS-EPS/MAN/04/0033, available at: http://oiswww.eumetsat.org/WEBOPS/eps-pg/IASI-L2/IASIL2-PG-0TOC.htm, (last access: 14 April 2014), 2004.

Folberth, G. A., Hauglustaine, D. A., Lathière, J., and Brocheton, F.: Interactive chemistry in the Laboratoire de Météorologie Dynamique general circulation model: model description and impact analysis of biogenic hydrocarbons on tropospheric chemistry, Atmos. Chem. Phys., 6, 2273–2319, doi:10.5194/acp-6-2273-2006, 2006.

Hauglustaine, D. A., Hourdin, F., Jourdain, L., Filiberti, M.-A., Walters, S., Lamarque, J.-F., and Holland, E. A.: Interactive chemistry in the Laboratoire de Meteorologie Dynamique general circulation model: description and background tropospheric chemistry evaluation, J. Geophys. Res., 109, D04314, doi:10.1029/2003JD003957, 2004.

Hilton, F., Armante, R., August, T., Barnet, C., Bouchard, A., Camy-Peyret, C., Capelle, V., Clarisse, L., Clerbaux, C., Coheur, P.-F., Collard, A., Crevoisier, C., Dufour, G., Edwards, D., Faijan, F., Fourrié, N., Gambacorta, A., Goldberg, M., Guidard, V., Hurtmans, D., Illingworth, S., Jacquinet-Husson, N., Kerzenmacher, T., Klaes, D., Lavanant, L., Masiello, G., Matricardi, M., McNally, A., Newman, S., Pavelin, E., Payan, S., Péquignot, E., Peyridieu, S.,

ACPD
14, 9975–10024, 2014

Phulpin, T., Remedios, J., Schlüssel, P., Serio, C., Strow, L., Stubenrauch, C., Taylor, J., Tobin, D., Wolf, W., and Zhou, D.: Hyperspectral earth observation from IASI: five years of accomplishments, B. Am. Meteorol. Soc., 93, 347–370, doi:10.1175/BAMS-D-11-00027.1, 2012.

Hirsch, A. I., Michalak, A. M., Bruhwiler, L. M., Peters, W., Dlugokencky, E. J., and Tans, P. P.: Inverse modeling estimates of the global nitrous oxide surface flux from 1998–2001, Global Biogeochem. Cy., 20, GB1008, doi:10.1029/2004GB002443, 2006.

Hourdin, F., Musat, I., Bony, S., Braconnot, P., Codron, F., Dufresne, J.-L., Fairhead, L., Filiberti, M.-A., Friedlingstein, P., Grandpeix, J.-Y., Krinner, G., LeVan, P., Li, Z.-X., and Lott, F.: The LMDZ4 general circulation model: climate performance and sensitivity to parametrized physics with emphasis on tropical convection, Clim. Dynam., 27, 787–813, doi:10.1007/s00382-006-0158-0, 2006.

Huszar, P., Teyssèdre, H., Michou, M., Voldoire, A., Olivié, D. J. L., Saint-Martin, D., Cariolle, D., Senesi, S., Salas Y Melia, D., Alias, A., Karcher, F., Ricaud, P., and Halenka, T.: Modeling the present and future impact of aviation on climate: an AOGCM approach with online coupled chemistry, Atmos. Chem. Phys., 13, 10027–10048, doi:10.5194/acp-13-10027-2013, 2013.

Imasu, R., Saitoh, N., and Niwa, Y.: Retrieval performance of GOSAT thermal infrared FTS sensor for measuring CO_2 concentrations, Proc. SPIE 6744, Sensors, Systems, and Next-Generation Satellites XI, 67440F, doi:10.1117/12.737796, 2007.

IPCC: Climate change 2007: The physical science basis, Contribution of working group I to the fourth assessment report of the intergovernmental panel on climate change, Cambridge, UK and New York, USA, Cambridge University Press, 996 pp., 2007.

Joly, M. and Peuch, V.-H.: Objective classification of air quality monitoring sites over Europe, Atmos. Environ., 47, 111–123, doi:10.1016/j.atmosenv.2011.11.025, 2012.

Josse, B., Simon, P., and Peuch, V.-H.: Rn-222 global simulations with the multiscale CTM MOCAGE, Tellus B, 56, 339–356, 2004.

Kallos, G., Astitha, M., Katsafados, P., and Spyrou, C.: Long-Range Transport of Anthropogenically and Naturally Produced Particulate Matter in the Mediterranean and North Atlantic: current State of Knowledge, J. Appl. Meteorol. Clim., 46, 1230–1251, 2007.

Krinner, G., Viovy, N., de Noblet-Ducoudré, N., Ogée, J., Polcher, J., Friedlingstein, P., Ciais, P., Sitch, S., and Prentice, I. C.: A dynamic global vegetation model for studies of the coupled atmosphere-biosphere system, Global Biogeochem. Cy., 19, GB1015, doi:10.1029/2003GB002199, 2005.

ACPD
14, 9975–10024, 2014

Kuze, A., Suto, H., Nakajima, M., and Hamazaki, T.: Thermal and near infrared sensor for carbon observation Fourier-transform spectrometer on the Greenhouse Gases Observing Satellite for greenhouse gases monitoring, Appl. Optics, 48, 6716–6733, 2009.

Lamarque, J.-F., Kyle, G. P., Meinshausen, M., Riahi, K., Smith, S. J., van Vuuren, D. P., Conley, A. J., and Vitt, F.: Global and regional evolution of short-lived radiatively-active gases and aerosols in the Representative Concentration Pathways, Climatic Change, 109, 191–212 doi:10.1007/s10584-011-0155-0, 2011.

Lamarque, J.-F., Shindell, D. T., Josse, B., Young, P. J., Cionni, I., Eyring, V., Bergmann, D., Cameron-Smith, P., Collins, W. J., Doherty, R., Dalsoren, S., Faluvegi, G., Folberth, G., Ghan, S. J., Horowitz, L. W., Lee, Y. H., MacKenzie, I. A., Nagashima, T., Naik, V., Plummer, D., Righi, M., Rumbold, S. T., Schulz, M., Skeie, R. B., Stevenson, D. S., Strode, S., Sudo, K., Szopa, S., Voulgarakis, A., and Zeng, G.: The Atmospheric Chemistry and Climate Model Intercomparison Project (ACCMIP): overview and description of models, simulations and climate diagnostics, Geosci. Model Dev., 6, 179–206, doi:10.5194/gmd-6-179-2013, 2013.

Lefèvre, F., Brasseur, G. P., Folkins, I., Smith, A. K., and Simon, P.: Chemistry of the 1991–1992 stratospheric winter: three-dimensional model simulations, J. Geophys. Res., 99, 9183–8195, 1994.

Lelieveld, J., Berresheim, H., Borrmann, S., Crutzen, P. J., Dentener, F. J., Fischer, H., Feichter, J., Flatau, P. J., Heland, J., Holzinger, R., Korrmann, R., Lawrence, M. G., Levin, Z., Markowicz, K. M., Mihalopoulos, N., Minikin, A., Ramanathan, V., de Reus, M., Roelofs, G. J., Scheeren, H. A., Sciare, J., Schlager, H., Schultz, M., Siegmund, P., Steil, B., Stephanou, E. G., Stier, P., Traub, M., Warneke, C., Williams, J., and Ziereis, H.: Global air pollution crossroads over the Mediterranean, Science, 298, 5594, 794–799, doi:10.1126/science.1075457, 2002.

Liu, J. J., Jones, D. B. A., Worden, J. R., Noone, D., Parrington, M., and Kar, J.: Analysis of the summertime buildup of tropospheric ozone abundances over the Middle East and North Africa as observed by the tropospheric emission spectrometer instrument, J. Geophys. Res., 114, D05304, doi:10.1029/2008JD010993, 2009.

Masson, O., Piga, D., Gurriaran, R., and D'Amico, D.: Impact of an exceptional Saharan dust outbreak in France: PM_{10} and artificial radionuclides concentrations in air and in dust deposit, Atmos. Environ., 44, 20, 2478–2486, doi:10.1016/j.atmosenv.2010.03.004, 2010.

ACPD
14, 9975–10024, 2014

Michou, M. and Peuch, V.-H.: Surface exchanges in the MOCAGE multiscale Chemistry and Transport Model, J. Water Sci., 15, 173–203, 2002.
Michou, M., Saint-Martin, D., Teyssèdre, H., Alias, A., Karcher, F., Olivié, D., Voldoire, A., Josse, B., Peuch, V.-H., Clark, H., Lee, J. N., and Chéroux, F.: A new version of the CNRM Chemistry-Climate Model, CNRM-CCM: description and improvements from the CCMVal-2 simulations, Geosci. Model Dev., 4, 873–900, doi:10.5194/gmd-4-873-2011, 2011.
Millán, M. M., Salvador, R., Mantilla, E., and Kallos, G.: Photooxidant dynamics in the Mediterranean basin in summer: results from European research projects, J. Geophys. Res., 102, 8811–8823, doi:10.1029/96JD03610, 1997.
Moss, R. H., Edmonds, J. A., Hibbard, K., Carter, T., Emori, S., Kainuma, M., Kram, T., Manning, M., Meehl, J., Mitchell, J., Nakicenovic, N., Riahi, K., Rose, S., Smith, S. J., Stouffer, R., Thomson, A. M., VanVuuren, D., Weyant, J., and Wilbanks, T.: Representative concentration pathways: a new approach to scenario development for the IPCC fifth assessment report, Nature, 463, 747–756, 2010.
Nabat, P., Solmon, F., Mallet, M., Kok, J. F., and Somot, S.: Dust emission size distribution impact on aerosol budget and radiative forcing over the Mediterranean region: a regional climate model approach, Atmos. Chem. Phys., 12, 10545–10567, doi:10.5194/acp-12-10545-2012, 2012.
Park, M., Randel, W. J., Emmons, L. K., and Livesey, N. J.: Transport pathways of carbon monoxide in the Asian summer monsoon diagnosed from Model of Ozone and Related Tracers (MOZART), J. Geophys. Res., 114, D08303, doi:10.1029/2008JD010621, 2009.
Peuch, V.-H., Amodei, M., Barthet, T., Cathala, M.-L., Josse, B., Michou, M., and Simon, P.: MOCAGE: Modèle de Chimie, Atmosphérique A Grande Echelle, Actes des Atelier de Modélisation de l'Atmosphère, Météo-France, 33–36, 1999.
Pfister, G., Petron, G., Emmons, L. K., Gille, J. C., Edwards, D. P., Lamarque, J.-F., J.-L. Attié, C. Granier, and Novelli, P. C: Evaluation of CO simulations and the analysis of the CO budget for Europe, J. Geophys. Res.-Atmos., 109, 2004.
Ramanathan, V. and Carmichael, G.: Global and regional climate changes due to black carbon, Nat. Geosci., 1, 221–227, doi:10.1038/ngeo156, 2008.
Randel, W. J. and Park, M.: Deep convective influence on the Asian summer monsoon anticyclone and associated tracer variability observed with Atmospheric Infrared Sounder (AIRS), J. Geophys. Res., 111, D12314, doi:10.1029/2005JD006490, 2006.

ACPD
14, 9975–10024, 2014

Razavi, A., Clerbaux, C., Wespes, C., Clarisse, L., Hurtmans, D., Payan, S., Camy-Peyret, C., and Coheur, P. F.: Characterization of methane retrievals from the IASI space-borne sounder, Atmos. Chem. Phys., 9, 7889–7899, doi:10.5194/acp-9-7889-2009, 2009.

Ricaud, P., Attié, J.-L., Teyssèdre, H., El Amraoui, L., Peuch, V.-H., Matricardi, M., and Schluessel, P.: Equatorial total column of nitrous oxide as measured by IASI on MetOp-A: implications for transport processes, Atmos. Chem. Phys., 9, 3947–3956, doi:10.5194/acp-9-3947-2009, 2009.

Rodgers, C. D.: Inverse Methods for Atmospheric Sounding: Theory and Practice, 1st edn., World Scientific, Singapore, 2000.

Rodwell, M. J. and Hoskins, B. J.: Monsoons and the dynamics of deserts, Q. J. Roy. Meteor. Soc., 122, 1385–1404, 1996.

Rudich, Y., Kaufman, Y. J., Dayan, U., Yu, H., and Kleidman, R. G.: Estimation of transboundary transport of pollution aerosols by remote sensing in the eastern Mediterranean, J. Geophys. Res.-Atmos., 113, 2008.

Saitoh, N., Touno, M., Hayashida, S., Imasu, R., Shiomi, K., Yokota, T., Yoshida, Y., Machida, T., Matsueda, H., and Sawa, Y.: Comparisons between XCH_4 from GOSAT Shortwave and Thermal Infrared Spectra and Aircraft CH_4 Measurements over Guam, SOLA, 8, 145–149, doi:10.2151/sola.2012-036, 2012.

Schicker, I., Radanovics, S., and Seibert, P.: Origin and transport of Mediterranean moisture and air, Atmos. Chem. Phys., 10, 5089–5105, doi:10.5194/acp-10-5089-2010, 2010.

Scheeren, H. A., Lelieveld, J., Roelofs, G. J., Williams, J., Fischer, H., de Reus, M., de Gouw, J. A., Warneke, C., Holzinger, R., Schlager, H., Klüpfel, T., Bolder, M., van der Veen, C., and Lawrence, M.: The impact of monsoon outflow from India and Southeast Asia in the upper troposphere over the eastern Mediterranean, Atmos. Chem. Phys., 3, 1589–1608, doi:10.5194/acp-3-1589-2003, 2003.

Schlüssel, P., Hultberg, T. H., Phillips, P. L., August, T., and Calbet, X.: The operational IASI Level 2 Processor, Adv. Space Res., 36, 982–988, 2005.

Stockwell, W. R., Kirchner, F., Kuhn, M., and Seefeld, S.: A new mechanism for regional atmospheric chemistry modelling, J. Geophys. Res.-Atmos., 102, 25847–25879, 1997.

Susskind, J., Blaisdell, J. M., Iredell, L., and Keita, F.: Improved temperature sounding and quality control methodology using AIRS/AMSU data: the AIRS science team version 5 retrieval algorithm, IEEE Trans. Geosci. Remote, 49, 883–907, 2011.

ACPD
14, 9975–10024, 2014

Szopa, S., Balkanski, Y., Schulz, M., Bekki, S., Cugnet, D., Fortems-Cheiney, A., Turquety, S., Cozic, A., Déandreis, C., Hauglustaine, D., Idelkadi, A., Lathière, J., Lefèvre, F., Marchand, M., Vuolo, R., Yan, N., and Dufresne, J.-L.: Aerosol and ozone changes as forcing for climate evolution between 1850 and 2100, Clim. Dynam., 40, 2223–2250, doi:10.1007/s00382-012-1408-y, 2013.

Teyssèdre, H., Michou, M., Clark, H. L., Josse, B., Karcher, F., Olivié, D., Peuch, V.-H., Saint-Martin, D., Cariolle, D., Attié, J.-L., Nédélec, P., Ricaud, P., Thouret, V., van der A, R. J., Volz-Thomas, A., and Chéroux, F.: A new tropospheric and stratospheric Chemistry and Transport Model MOCAGE-Climat for multi-year studies: evaluation of the present-day climatology and sensitivity to surface processes, Atmos. Chem. Phys., 7, 5815–5860, doi:10.5194/acp-7-5815-2007, 2007.

Traub, M., Fischer, H., de Reus, M., Kormann, R., Heland, H., Ziereis, H., Schlager, H., Holzinger, R., Williams, J., Warneke, C., de Gouw, J., and Lelieveld, J.: Chemical characteristics assigned to trajectory clusters during the MINOS campaign, Atmos. Chem. Phys., 3, 459–468, doi:10.5194/acp-3-459-2003, 2003.

Turquety, S., Hadji-Lazaro, J., Clerbaux, C., Hauglustaine, D. A., Clough, S. A., Cassé, V., Schlüssel, P., and Mégie, G.: Operational trace gas retrieval algorithm for the Infrared Atmospheric Sounding Interferometer, J. Geophys. Res., 109, D21301, doi:10.1029/2004JD004821, 2004.

van der Werf, G. R., Randerson, J. T., Collatz, G. J., and Giglio, L.: Carbon emissions from fires in tropical and subtropical ecosystems, Glob. Change Biol., 9, 547–562, 2003.

Voldoire, A., Sanchez-Gomez, E., Salas y Melia, D., Decharme, B., Cassou, C., Sénési, S., Valcke, S., Beau, I., Alias, A., Chevallier, M., Deque, M., Deshayes, J., Douville, H., Fernandez, E., Madec, G., Maisonnave, E., Moine, M.-P., Planton, S., Saint-Martin, D., Szopa, S., Tyteca, S., Alkama, R., Belamari, S., Braun, A., Coquart, L., and Chauvin, F.: The CNRM-CM5.1 global climate model: description and basic evaluation, Clim. Dynam., 40, 2091–2121, doi:10.1007/s00382-011-1259-y, 2013.

Wanger, A., Peleg, M., Sharf, G., Mahrer, Y., Dayan, U., Kallos, G., Kotroni, V., Lagouvardos, K., Varinou, M., Papadopoulos, A., and Luria, M.: Some observational and modelling evidence of long range transport of air pollutants from Europe towards the Israeli Coast, J. Geophys. Res., 105, 7177–7186, 2000.

Waugh, D. W. and Hall, T.: Age of stratospheric air: theory, observatiosn and models, Rev. Geophys., 40, 1010, doi:10.1029/2000RG000101, 2002.

ACPD
14, 9975–10024, 2014

Worden, J., Kulawik, S., Frankenberg, C., Payne, V., Bowman, K., Cady-Peirara, K., Wecht, K., Lee, J.-E., and Noone, D.: Profiles of CH_4, HDO, H_2O, and N_2O with improved lower tropospheric vertical resolution from Aura TES radiances, Atmos. Meas. Tech., 5, 397–411, doi:10.5194/amt-5-397-2012, 2012.

World Meteorological Organization, Scientific assessment of ozone depletion: 1998, Rep. 44, Geneva, Switzerland, 1998.

Wunch, D., Toon, G. C., Wennberg, P. O., Wofsy, S. C., Stephens, B. B., Fischer, M. L., Uchino, O., Abshire, J. B., Bernath, P., Biraud, S. C., Blavier, J.-F. L., Boone, C., Bowman, K. P., Browell, E. V., Campos, T., Connor, B. J., Daube, B. C., Deutscher, N. M., Diao, M., Elkins, J. W., Gerbig, C., Gottlieb, E., Griffith, D. W. T., Hurst, D. F., Jiménez, R., Keppel-Aleks, G., Kort, E. A., Macatangay, R., Machida, T., Matsueda, H., Moore, F., Morino, I., Park, S., Robinson, J., Roehl, C. M., Sawa, Y., Sherlock, V., Sweeney, C., Tanaka, T., and Zondlo, M. A.: Calibration of the Total Carbon Column Observing Network using aircraft profile data, Atmos. Meas. Tech., 3, 1351–1362, doi:10.5194/amt-3-1351-2010, 2010.

Xiong, X., Barnet, C., Maddy, E., Sweeney, C., Liu, X., Zhou, L., and Goldberg, M.: Characterization and validation of methane products from the Atmospheric Infrared Sounder (AIRS), J. Geophys. Res., 113, G00A01, doi:10.1029/2007JG000500, 2008.

Yokota, T., Yoshida, Y., Eguchi, N., Ota, Y., Tanaka, T., Watanabe, H., and Maksyutov, S.: Global concentrations of CO_2 and CH_4 retrieved from GOSAT: first preliminary results, SOLA, 5, 160–163, doi:10.2151/sola.2009-041, 2009.

Yoshida, Y., Kikuchi, N., Morino, I., Uchino, O., Oshchepkov, S., Bril, A., Saeki, T., Schutgens, N., Toon, G. C., Wunch, D., Roehl, C. M., Wennberg, P. O., Griffith, D. W. T., Deutscher, N. M., Warneke, T., Notholt, J., Robinson, J., Sherlock, V., Connor, B., Rettinger, M., Sussmann, R., Ahonen, P., Heikkinen, P., Kyrö, E., Mendonca, J., Strong, K., Hase, F., Dohe, S., and Yokota, T.: Improvement of the retrieval algorithm for GOSAT SWIR XCO_2 and XCH_4 and their validation using TCCON data, Atmos. Meas. Tech., 6, 1533–1547, doi:10.5194/amt-6-1533-2013, 2013.

Ziv, B., Saaroni, H., and Alpert, P.: The factors governing the summer regime of the eastern Mediterranean, Int. J. Climatol., 24, 1859–1871, doi:10.1002/joc.1113, 2004.

ACPD
14, 9975–10024, 2014

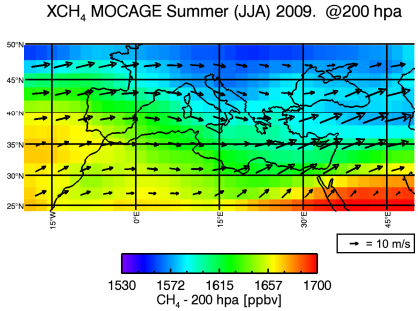

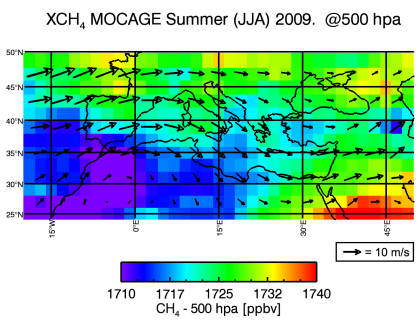

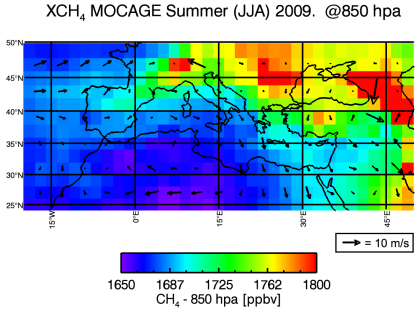

ACPD
14, 9975–10024, 2014

Variability of tropospheric methane above the Mediterranean Basin

P. Ricaud et al.

Fig. 1. (From bottom to top) Fields of CH_4 as calculated by MOCAGE and averaged for summer (JJA) 2009 at 850, 500 and 200 hPa. Superimposed are the horizontal winds from ARPEGE averaged over the same period. In order to highlight the CH_4 horizontal gradients, the range of the colour scale changes from top to bottom.

ACPD
14, 9975–10024, 2014

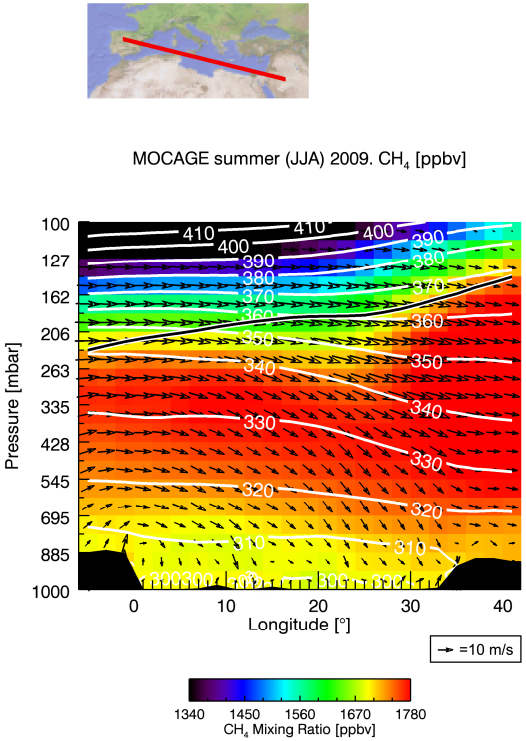

Fig. 2. Vertical distribution of CH_4 as calculated by MOCAGE and averaged for JJA 2009 as a function of longitude along the red line represented above the Figure. Superimposed are the associated longitudinal and vertical winds from ARPEGE, together with the isentropes (white lines) and the cold point tropopause from NOAA/NCEP reanalyses (black line) averaged over the same period.

ACPD
14, 9975–10024, 2014

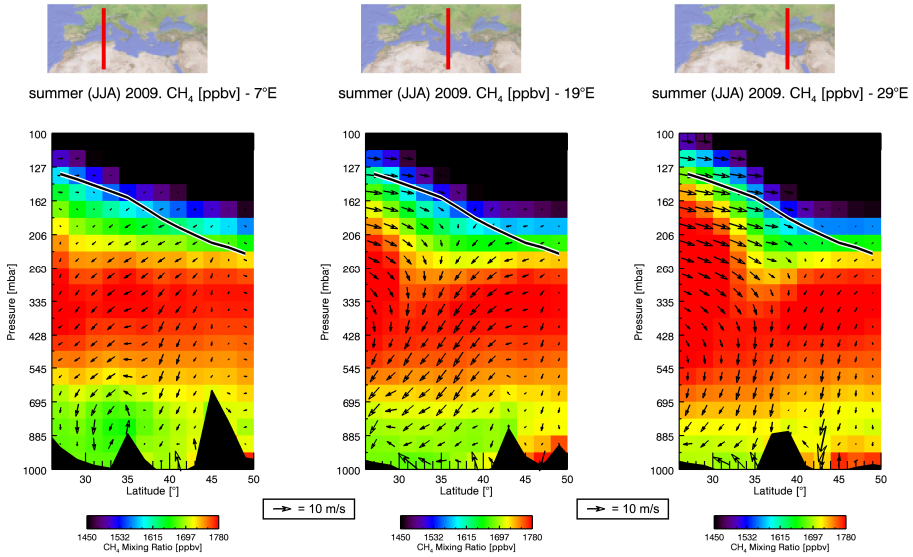

Fig. 3. (From left to right) Vertical distribution of CH_4 as calculated by MOCAGE and averaged for JJA 2009 as a function of latitude along 3 different longitudes: 7° E, 19° E and 29° E, represented by a red line on the map above each Figure. Superimposed are the associated latitudinal and vertical winds from ARPEGE, together with the cold point tropopause from NOAA/NCEP reanalyses (black line) averaged over the same period.

ACPD
14, 9975–10024, 2014

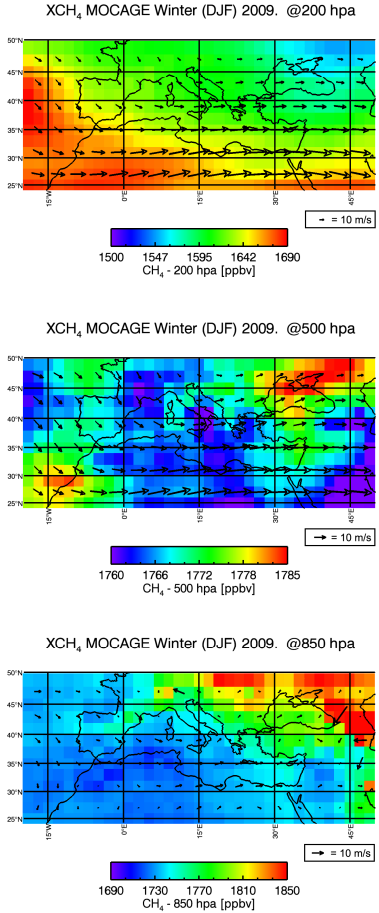

Fig. 4. Same as Fig. 1, but for winter (DJF) 2009.

ACPD
14, 9975–10024, 2014

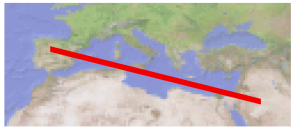

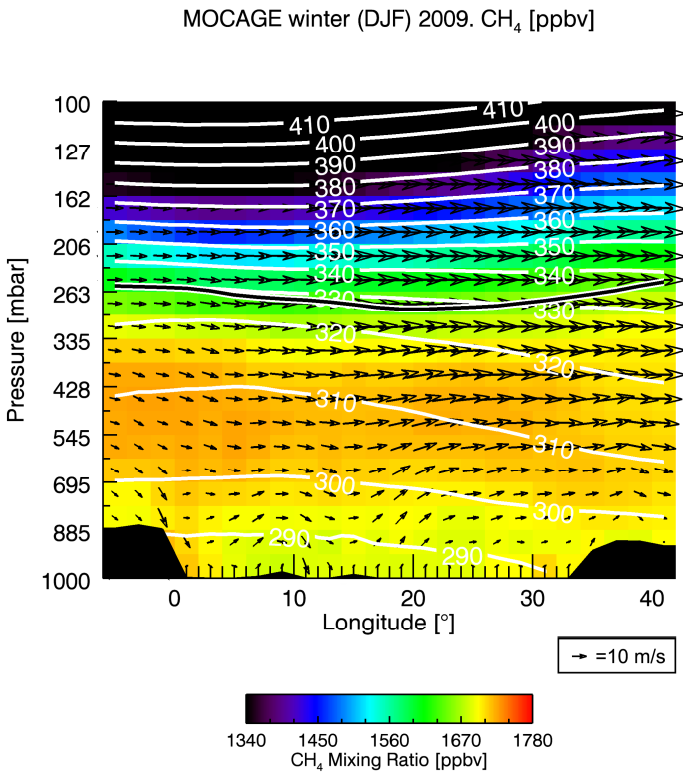

Fig. 5. Same as Fig. 2, but for winter (DJF) 2009.

ACPD
14, 9975–10024, 2014

Variability of tropospheric methane above the Mediterranean Basin

P. Ricaud et al.

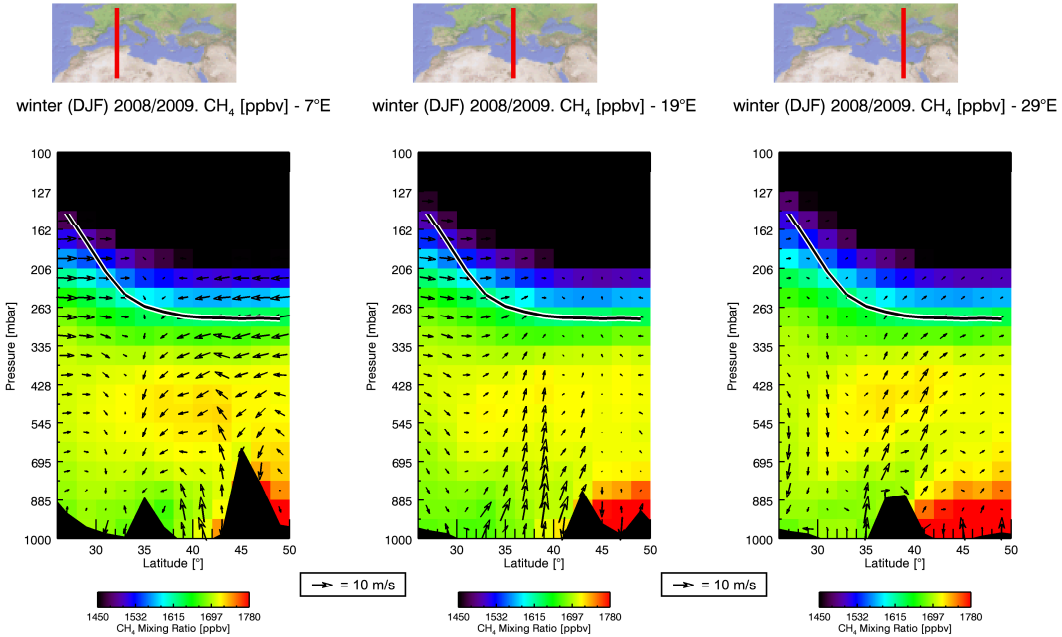

Fig. 6. Same as Fig. 3, but for winter (DJF) 2009.

ACPD
14, 9975–10024, 2014

Variability of tropospheric methane above the Mediterranean Basin

P. Ricaud et al.

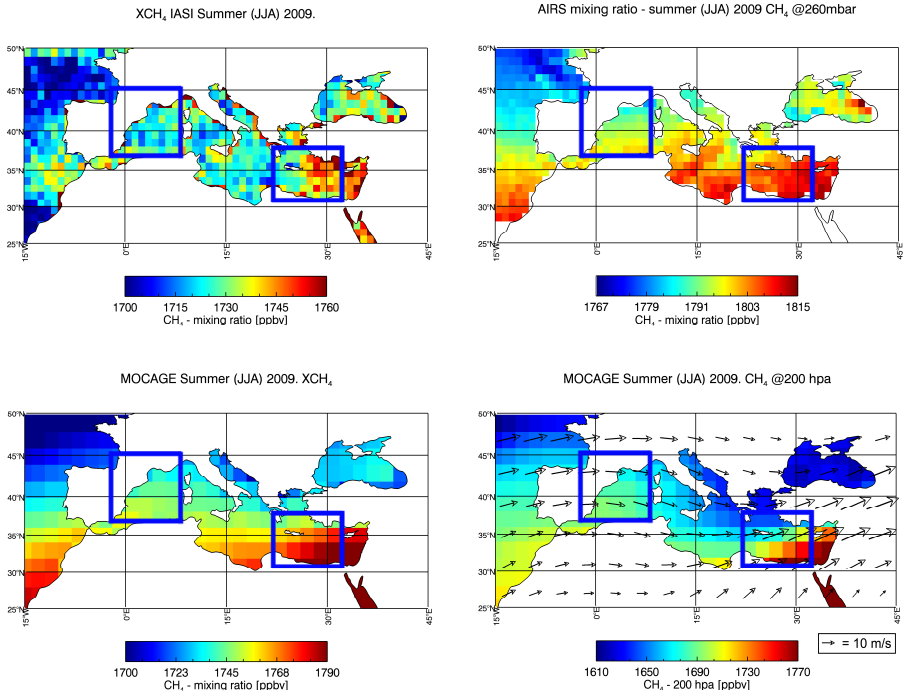

Fig. 7. Field of total columns of CH_4 as measured by IASI and averaged for summer (JJA) 2009 (top left), and field of CH_4 at 260 hPa as measured by AIRS and averaged for JJA 2009 (top right). (Bottom) Same as above but as calculated by MOCAGE. Satellite data are represented in a $1^\circ \times 1^\circ$ resolution whilst model data are shown in a $2^\circ \times 2^\circ$ resolution. The two blue squares in the lower left Figure represent the Western and Eastern Mediterranean Basins where the measured and modelled data are selected over the Mediterranean Sea. Superimposed are the horizontal winds from ARPEGE at 200 hPa averaged over the same period (bottom right). In order to highlight the CH_4 horizontal gradients, the range of the colour scale changes for each figure.

ACPD
14, 9975–10024, 2014

Variability of tropospheric methane above the Mediterranean Basin

P. Ricaud et al.

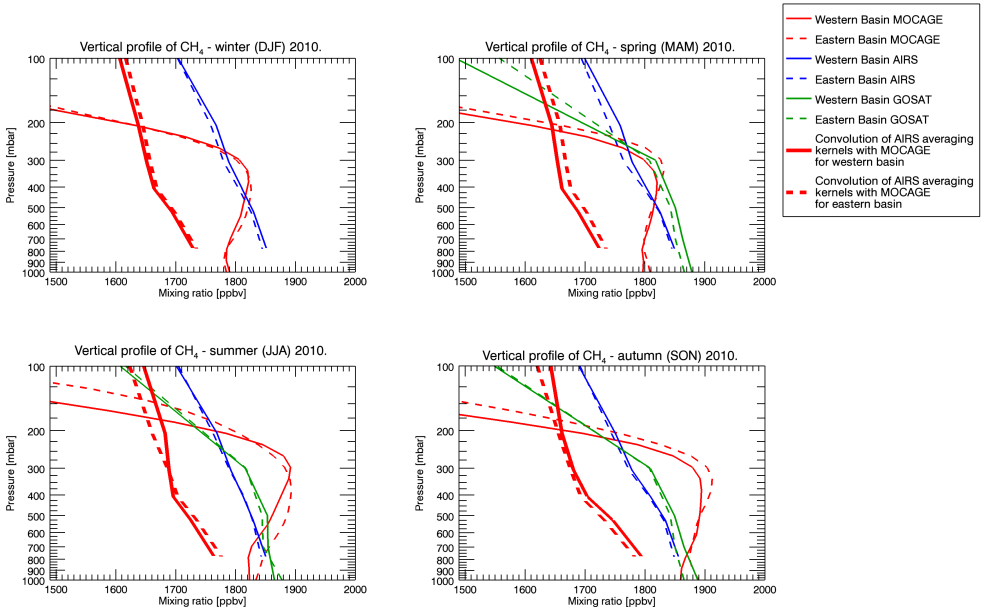

Fig. 8. (From top to bottom and from left to right) Seasonally-averaged vertical profiles of CH_4 as measured by AIRS (blue lines) and GOSAT (green lines), and as calculated by MOCAGE (thin red lines) over the Eastern (dashed lines) and Western (solid lines) MBs in winter, summer, spring and autumn 2010. Also shown are the seasonally-averaged MOCAGE profiles convolved with the AIRS averaging kernels (thick red lines) for the four seasons over the Eastern (dashed lines) and Western (solid lines) MBs.

ACPD
14, 9975–10024, 2014

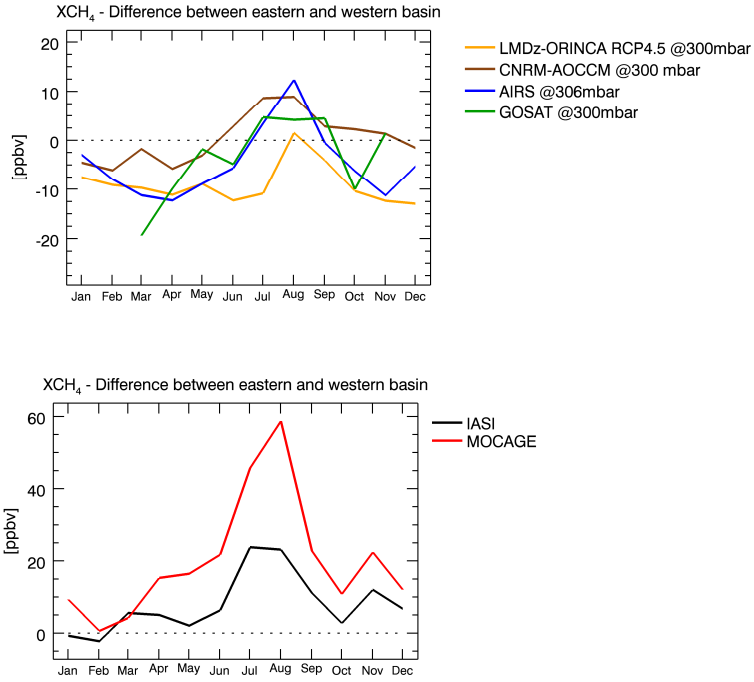

Fig. 9. (Top) Seasonal evolution of the difference in the CH_4 fields between the Eastern and Western MB as measured by AIRS (blue line) and GOSAT (green line) at 306 and 300 hPa, respectively and as calculated by LMDz-OR-INCA (yellow line) and CNRM-AOCCM (brown line). (Bottom) Seasonal evolution of the difference in the CH_4 total columns between the Eastern and Western MB as measured by IASI (black line) and as calculated by MOCAGE (red line). The LMDz-OR-INCA and CNRM-AOCCM data sets cover the climatological period 2001–2010. The MOCAGE and IASI data sets cover the period 2008–2011 whilst the satellite AIRS and GOSAT data sets are representative of the year 2010.

ACPD
14, 9975–10024, 2014

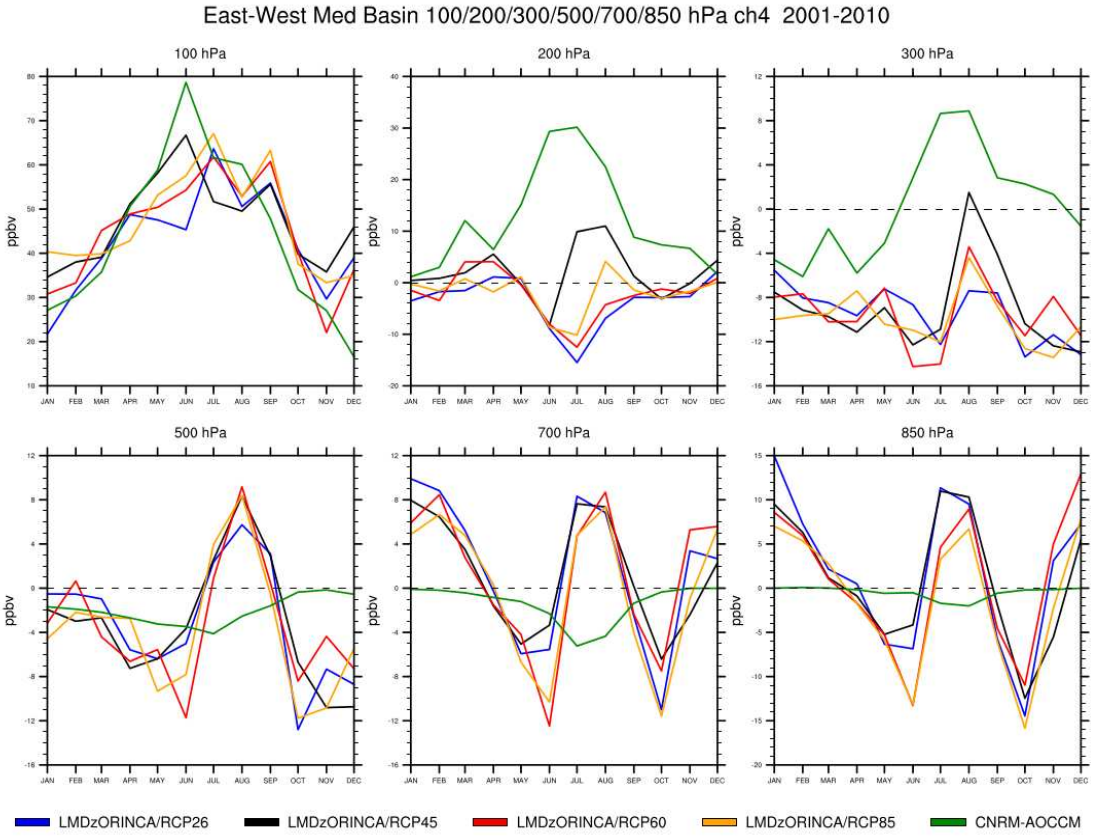

Fig. 10. (From top to bottom and from left to right) Seasonal evolution of the difference in the CH_4 fields between the Eastern and Western MB over the climatological period 2001–2010 at 100, 200, 300, 500, 700 and 850 hPa as calculated by CNRM-AOCCM (green) model and LMDz-OR-INCA according to the 4 IPCC scenarios: RPCs 2.6 (blue), 4.5 (black), 6.0 (red) and 8.5 (yellow). See Sect. 2.2 for more details.

ACPD
14, 9975–10024, 2014

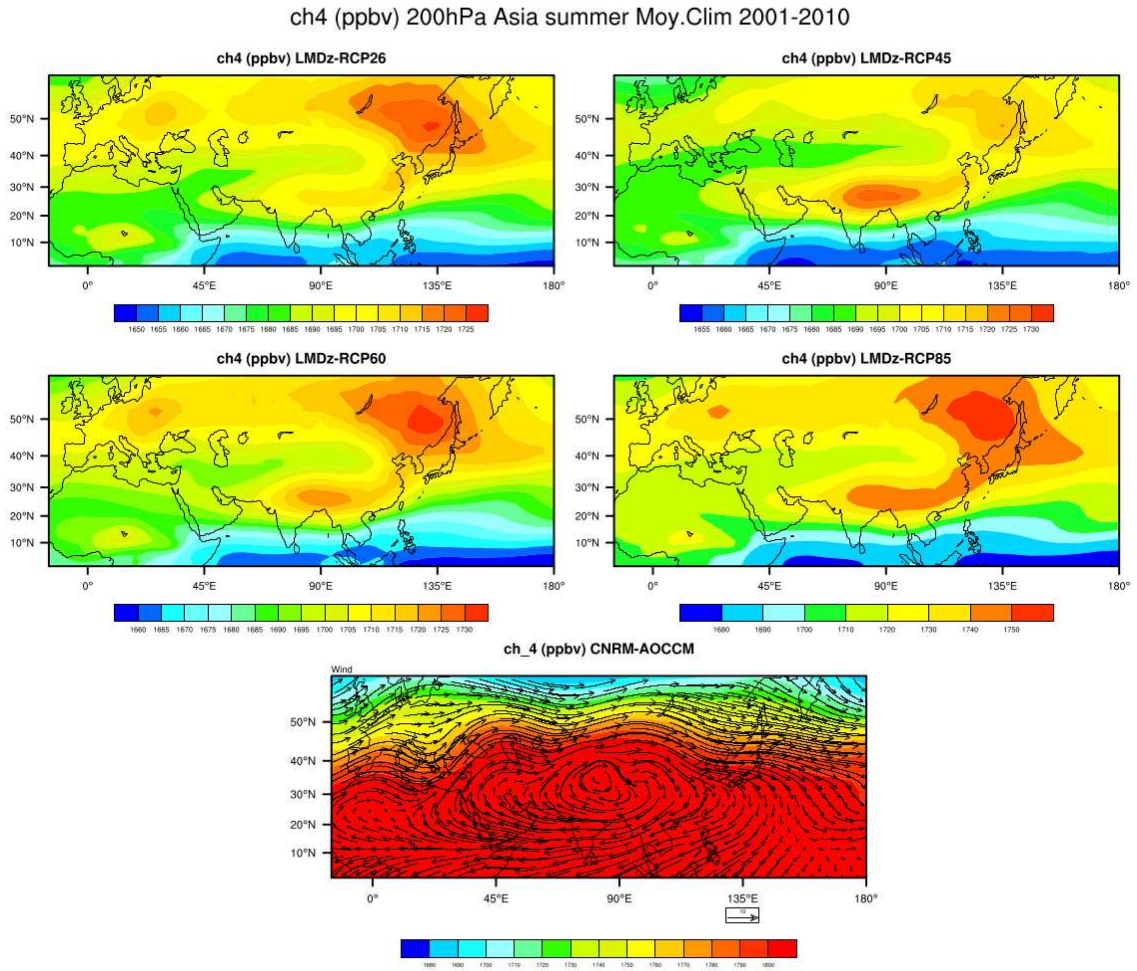

ACPD
14, 9975–10024, 2014

Variability of tropospheric methane above the Mediterranean Basin

P. Ricaud et al.

Fig. 11. Fields of CH_4 as calculated by the CNRM-AOCCM model (bottom) and the LMDz-OR-INCA model (top and centre) considering the 4 IPCC scenarios (RCPs 2.6 (top left), 4.5 (top right), 6.0 (centre left) and 8.5 (centre right)) at 200 hPa averaged over the summer season (JJA) and the climatological period 2001–2010. Superimposed to the CNRM-AOCCM CH_4 fields (bottom) is the wind field at 200 hPa averaged over the same period. Note that the range of the colour scale changes for each figure.

ACPD
14, 9975–10024, 2014

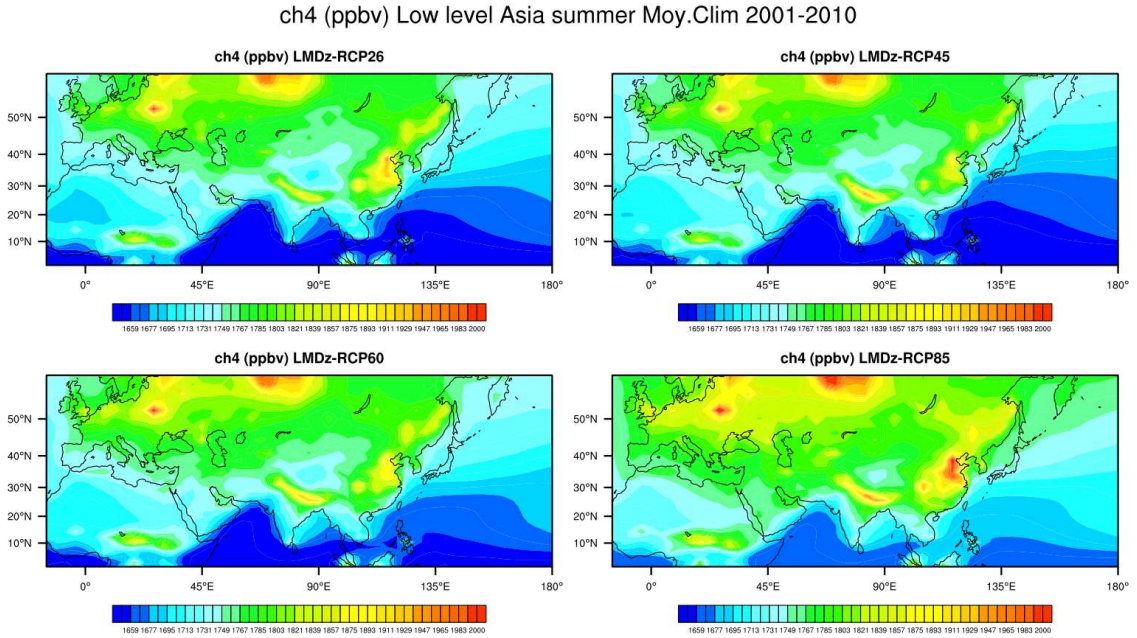

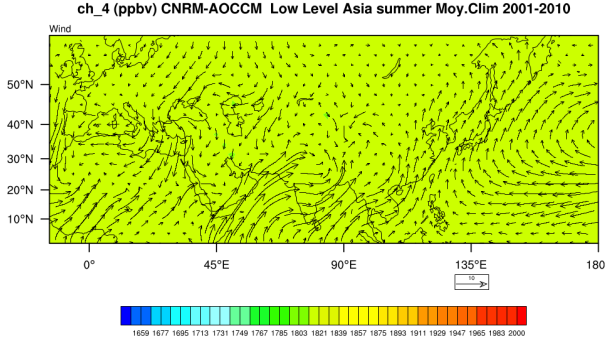

ACPD
14, 9975–10024, 2014

Variability of tropospheric methane above the Mediterranean Basin

P. Ricaud et al.

Fig. 12. Fields of surface CH_4 as calculated by the CNRM-AOCCM model (bottom) and the LMDz-OR-INCA model (top and centre) according to the 4 IPCC scenarios (RCPs 2.6 (top left), 4.5 (top right), 6.0 (centre left) and 8.5 (centre right)) averaged over the summer season (JJA) and the climatological period 2001–2010. Superimposed to the CNRM-AOCCM CH_4 fields (bottom) is the surface wind field averaged over the same period. Note that the range of the colour scale changes for each figure.

ACPD
14, 9975–10024, 2014